2015

Energy Harvesting toward the Vibration Reduction of Turbomachinery Blades via Resonance Frequency Detuning

Taylor Hynds
University of Central Florida

ENERGY HARVESTING TOWARD THE VIBRATION REDUCTION OF TURBOMACHINERY BLADES VIA RESONANCE FREQUENCY DETUNING

by

TAYLOR D. HYNDS
B.S. Florida State University, 2013

A thesis submitted in partial fulfillment of the requirements
for the degree of Master of Science
in the Department of Mechanical and Aerospace Engineering
in the College of Engineering and Computer Science
at the University of Central Florida
Orlando, Florida

Summer Term
2015

Major Professor: Jeffrey L. Kauffman

ABSTRACT

Piezoelectric-based energy harvesting devices provide an attractive approach to powering remote devices as ambient mechanical energy from vibrations is converted to electrical energy. These devices have numerous potential applications, including actuation, sensing, structural health monitoring, and vibration control – the latter of which is of particular interest here. This work seeks to develop an understanding of energy harvesting behavior within the framework of a semi-active technique for reducing turbomachinery blade vibrations, namely resonance frequency detuning. In contrast with the bulk of energy harvesting research, this effort is not focused on maximizing the power output of the system, but rather providing the low power levels required by resonance frequency detuning. The demands of this technique dictate that harvesting conditions will be far from optimal, requiring that many common assumptions in conventional energy harvesting research be relaxed.

Resonance frequency detuning has been proposed as a result of recent advances in turbomachinery blade design that have, while improving their overall efficiency, led to significantly reduced damping and thus large vibratory stresses. This technique uses piezoelectric materials to control the stiffness, and thus resonance frequency, of a blade as the excitation frequency sweeps through resonance. By detuning a structure's resonance frequency from that of the excitation, the overall peak response can be reduced, delaying high cycle fatigue and extending the lifetime of a blade.

Additional benefits include reduced weight, drag, and noise levels as reduced vibratory stresses allow for increasingly light blade construction.

As resonance frequency detuning is most effective when the stiffness states are well separated, it is necessary to harvested at nominally open- and short-circuit states, corresponding to the largest separation in stiffness states. This presents a problem from a harvesting standpoint however, as open- and short-circuit correspond to zero charge displacement and zero voltage, respectively, and thus there is no energy flow. It is, then, desirable to operate as near these conditions as possible while still harvesting sufficient energy to provide the power for state-switching. In this research a metric is developed to study the relationship between harvested power and structural stiffness, and a key result is that appreciable energy can be harvested far from the usual optimal conditions in a typical energy harvesting approach. Indeed, sufficient energy is available to power the on-blade control while essentially maintaining the desired stiffness states for detuning. Furthermore, it is shown that the optimal switch in the control law for resonance frequency detuning may be triggered by a threshold harvested power, requiring minimal on-blade processing. This is an attractive idea for implementing a vibration control system on-blade, as size limitations encourage removing the need for additional sensing and signal processing hardware.

ACKNOWLEDGMENTS

This work was supported by the Office of Naval Research under the supervision of Dr. Joseph Doychak, who I thank for making this effort possible. I would also like to thank Dr. Jeff Kauffman for his insights, guidance, and motivation. Finally, I would like to thank my family and close friends for their support through this endeavor, and indeed all that I do.

TABLE OF CONTENTS

LIST OF FIGURES

LIST OF TABLES

CHAPTER 1
INTRODUCTION

Innovation in turbomachinery blade construction has led to significant increases in their aerodynamic efficiency, in addition to reduced part counts, weight, and complexity. There is, however, a cost associated with these advances – namely, greatly reduced structural damping and in turn large vibratory stresses. Over time, these stresses can cause a blade to succumb to high cycle fatigue, potentially leading to crack propagation and ultimately catastrophic failure. In light of these issues, a vibration reduction approach is desired to alleviate large vibratory stresses and thus increase blade lifetime. One such approach, resonance frequency detuning, is of particular interest here. Resonance frequency detuning uses piezoelectric materials to tailor a blade's structural properties in an effort to avoid resonance conditions, thus limiting vibratory response. Implementation of this vibration reduction technique requires an on-blade power source to modify the electrical boundary conditions on the integrated piezoelectric material. Conveniently, the same piezoelectric material used for stiffness control may be used to harvest energy when the control system is not active. This work focuses on understanding the behavior of piezoelectric energy harvesting systems within the context of resonance frequency detuning. Note that this effort is currently being developed for the turbofan and cold side of the compressor, due to both the temperature limitations of piezoelectric

materials and the fact that the most significant issues with high cycle fatigue are observed in these regions [1].

1.1 Energy Harvesting

As advances continue in wireless, remote, and low power electronics and sensors, a concurrent effort focuses on developing methods that harvest energy in some form from the ambient environment and convert to electrical energy in an effort to improve battery life and reduce maintenance costs. There are a number of types of energy harvesting devices – photovoltaic, thermoelectric, hydroelectric, to name a few, and the desired type of conversion depends on the environment and application. This work is concerned with the conversion of mechanical energy from a vibrating source to electrical energy. Focusing on vibration energy sources, there are again several methods of energy conversion – including electromagnetic, electrostatic, and piezoelectric. Of these, piezoelectric-based techniques are of particular interest due to their direct conversion of mechanical strain energy to electrical energy and the relative simplicity of integrating piezoelectric materials in a structure. As such, there has been a great deal of work on the optimization of piezoelectric-based vibrational energy harvesting devices over the past decade, with a variety of different approaches to the problem being taken – for example, through material advances, optimization of system parameters, advanced harvesting circuitry, or seeking broadband solutions [2, 3, 4]. The energy harvesting aspect of this work, however, differs from typical energy harvesting research. The power required to implement resonance frequency detuning is minimal, as it only requires two switches per excitation. This

is in contrast to many vibration damping approaches which require as many as four switches per vibration cycle, a fact which may limit their use in the turbomachinery environment where excitation frequencies can be very high. Thus, we seek not to optimize the power output of the system but rather to develop an understanding of energy harvesting behavior under the conditions relevant to this application. For example, it is ideal to harvest at nominally open- and short-circuit conditions in resonance frequency detuning as this leads to the greatest vibration reduction, yet these cases are ignored in conventional energy harvesting research due to the inherently low flow of energy. It is therefore important to develop an understanding of the behavior of energy harvesting systems under these conditions, a topic which is studied here.

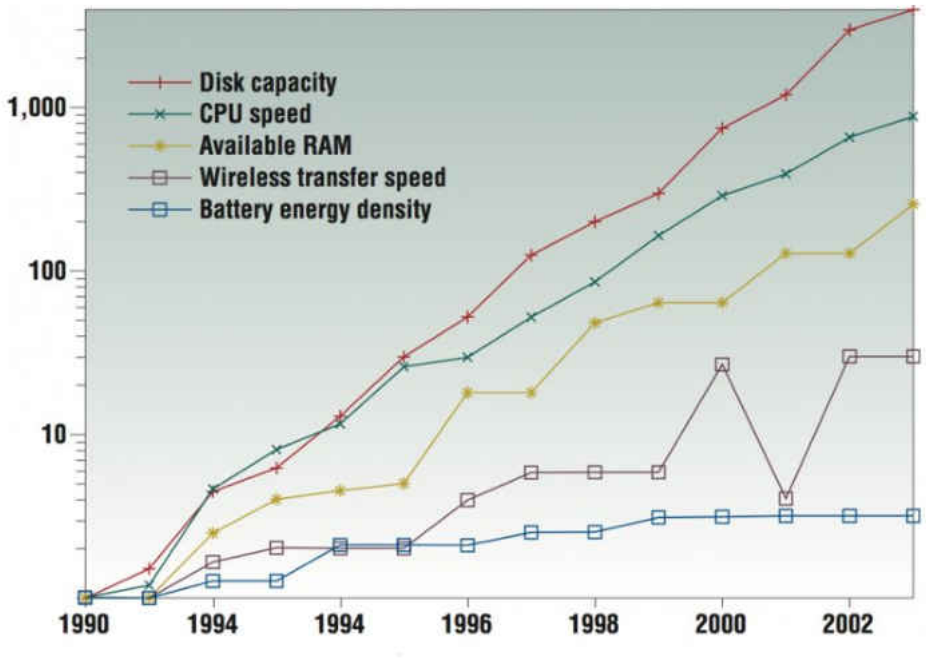

Figure 1.1: *Trends in battery and computer technology. From [5].*

Implementation of resonance frequency detuning in the rotating frame would require that the power source be located on the blade. Clearly the needed energy is present on-blade, as the purpose of this technique is to reduce blade vibrations and, conveniently, the piezoelectric material embedded in the blade for stiffness control would naturally convert strain energy to electrical energy, thus providing the required power source. An on-blade system also presents size limitations, making it desirable to minimize the need for additional hardware for sensing and signal processing. A natural solution would be to use the harvested energy, which must correlate with the blade vibrations due to the coupled electromechanical nature of piezoelectric materials, as a proxy for knowledge of the local vibration characteristics, thus eliminating the need for sensors and limiting any signal processing.

1.2 Turbomachinery Blade Vibrations

High rotations speeds as well as rotor-stator aerodynamic interactions in turbomachinery passages induce large periodic vibratory stresses, with the excitation frequency strongly dependent on the rotation speed. The aerodynamic forces due to rotor-stator interactions arise from the force required to turn the airflow as it moves alternatively between rotor and stator passages. Figure 1.2, a flow visualization from a CFD simulation, depicts how the airflow turns as it passes through a turbine. Other sources of periodic excitations include inlet guide vanes, or indeed any source of circumferential pressure variation in the flow field.

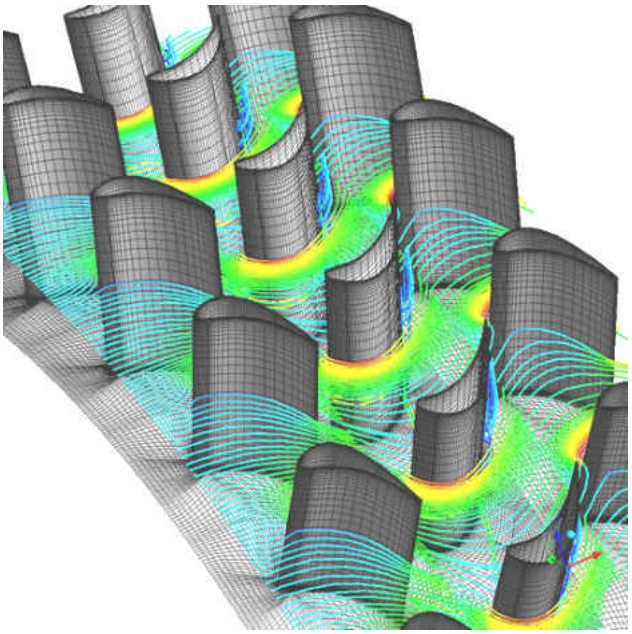

Figure 1.2: *Characteristic flow through a turbomachinery rotor-stator passage. From [6].*

Blade dynamics are further complicated by the effect of rotation speed on the blade resonance frequency, through geometric stiffening and softening effects [7]. The complex interaction between these effects is commonly displayed via the Campbell diagram, seen in Figure 1.3, where the blade resonance frequencies as well as excitation frequencies are shown as a function of rotation speed [8]. At speeds where these frequencies match, resonant vibrations are induced on the blade, resulting in large vibratory stresses. Turbomachinery are, of course, designed such that they do not nominally operate at blade resonance conditions, however it is inevitable that a number of modes will be excited as the rotation speed sweeps through a large range during start-up and shut-down. These fleeting excitations can, over time, lead to high-cycle fatigue, eventually causing the initiation and propagation of cracks, and ultimately catastrophic failure. An example of this can be seen in Figure 1.4. Catastrophic failure in a stage one compressor blisk row resulted in the forced in-flight

shut-down of an engine on a Saab 340B passenger aircraft [9]. The failure of the engine was related to high-frequency vibratory aerodynamic loading of the stage one compressor blisk, which resulted in the development of reverse-bending fatigue cracks in the blisk blades [9]. From examples such as this the need for a vibration damping system is made clear. In addition, such a system would allow for lighter and thinner blade construction due to reduced vibratory stresses over a blade's lifetime, and as a result an increase in aerodynamic efficiency and reduction in weight can be expected.

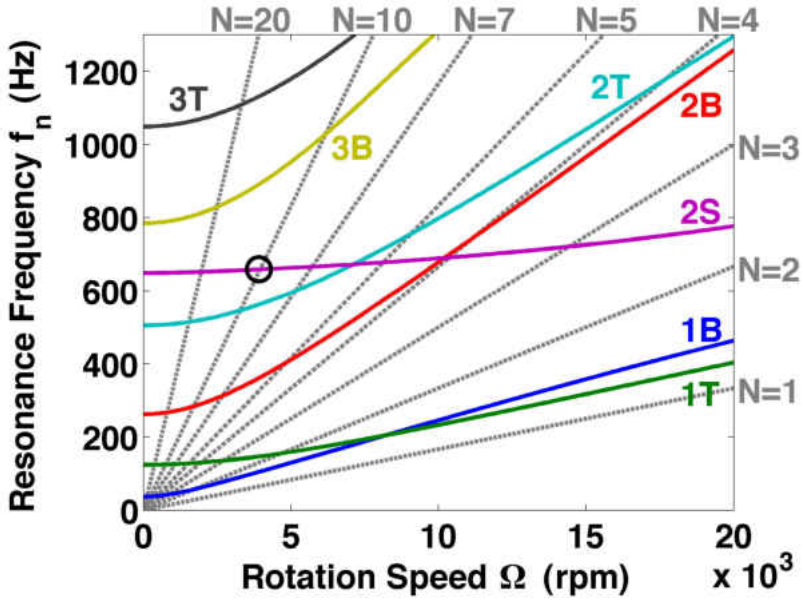

Figure 1.3: *Variation of natural frequencies (solid lines) due to rotation speed for a representative blade. Also depicted are the "speed lines," denoted by their engine order (dashed gray lines). From [8].*

Figure 1.4: *Failed first stage compressor row. From [9].*

1.2.1 Monolithic Bladed Disks

An effort to improve the aerodynamic efficiency of turbomachinery blades has led to their monolithic construction. In this turbomachinery blade construction method, the blades and hub are constructed as one piece; previously, the blades would be constructed separately from the hub and later attached (see Figures 1.5 and 1.6). This technique has the benefit of reducing the parts count as well as removing a source of drag where there would have previously been an attachment point; it does, however, remove a significant source of damping. The surfaces at the interface between the hub and the blade rub against one another, and the blade vibrations are damped as energy is dissipated

through friction. With monolithic blade construction this source of damping is removed; resonance frequency detuning seeks to provide an additional source of damping.

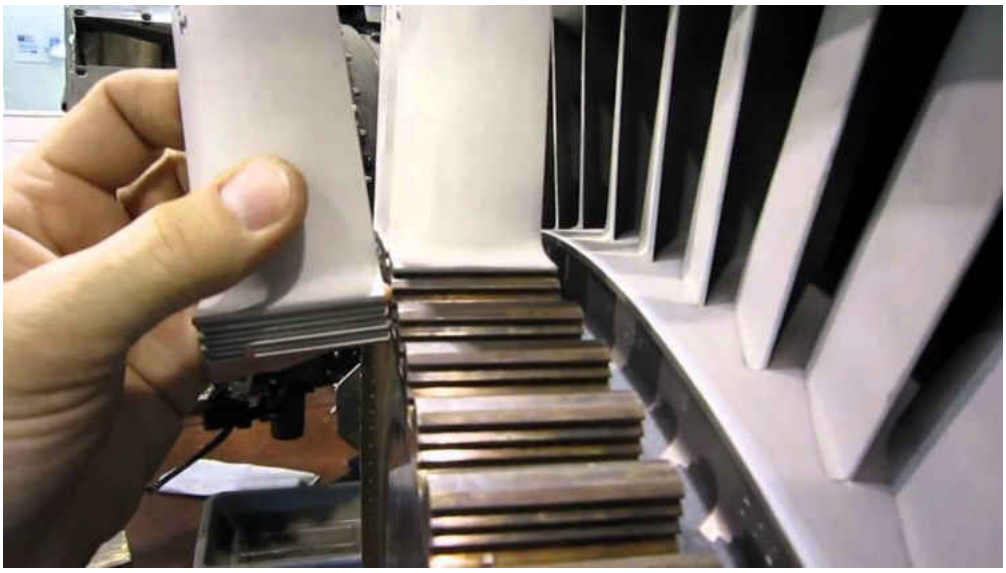

Figure 1.5: *Separate blade and hub construction. From [10].*

Figure 1.6: *Monolithic construction. From [11].*

1.3 Resonance Frequency Detuning

This research focuses on energy harvesting behavior in light of a vibration reduction technique of interest for turbomachinery applications, resonance frequency detuning. As discussed in the previous section, this vibration reduction effort is motivated in part by advances in turbomachinery blade manufacturing that have led to their monolithic construction and, while there are many advantages to this method of construction, it comes at the cost of significantly reduced damping due to the removed interface. As a result these blades are susceptible to large, high frequency vibratory stresses that can lead to high-cycle fatigue and ultimately catastrophic failure. Alternative methods of reducing turbomachinery blade vibrations are therefore needed.

Though a number of both passive and semi-active vibration damping methods are well established, many of these approaches are not well suited to the turbomachinery environment. Conventional approaches include adding a layer of viscoelastic material to a structure; these materials act as both a elastic solid and a viscous fluid – while they tend to retain a deformed configuration like a viscous fluid, they ultimately return to their original state just as an elastic solid [12]. Under ideal conditions viscoelastic materials provide a significant amount of damping, however their effectiveness is heavily dependent on frequency and temperature, diminishing their effectiveness in turbomachinery [13]. Passive piezoelectric-based approaches shunt the material with a circuit designed to dissipate the converted electrical energy, for example a resistive shunt or a resistive-inductive shunt [14, 15]. Effective performance of these approaches requires tuning the circuit parameters to the mechanical excitation that is targeted, often requiring additional branches to be

added to the circuit as additional modes are targeted. Turbomachinery blade vibration control systems must necessarily target a large number of modes, and the many additional circuit branches that would be required make passive approaches not compatible with the size limitations for embedding the device on-blade. Semi-active piezoelectric-based techniques can, however, provide significant vibration reduction over a wide spectrum of excitation frequencies and yet often require very little energy [13]. The drawback to many of these techniques is their complex switching requirements, often requiring as many as four switches per vibration cycle (see, for example, the depiction of state-switching in Figure 1.7) [16]. This high-frequency switching requires real-time detailed knowledge system's vibration characteristics, and the hardware required for sensing, processing, and switching may be prohibitive in the turbomachinery environment.

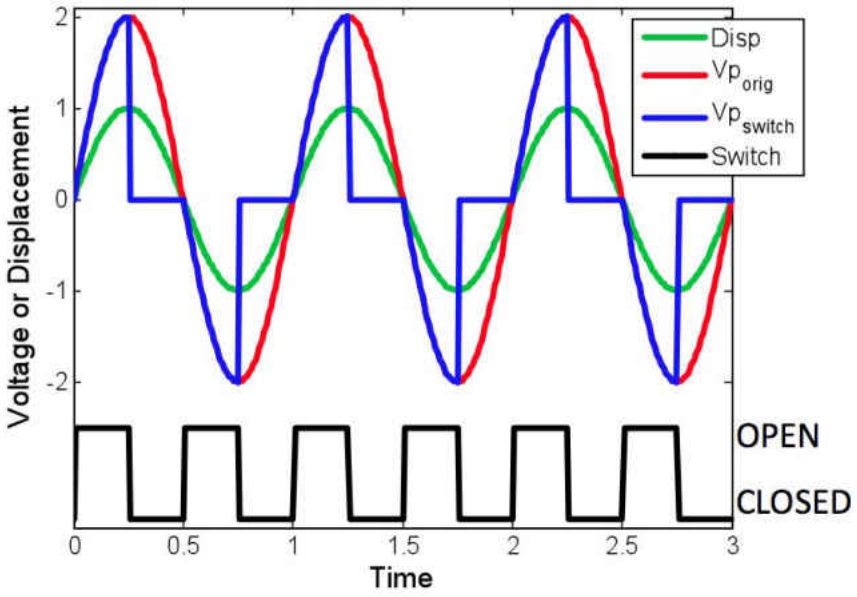

Figure 1.7: *State switching depicted through the displacement and piezoelectric voltage waveforms. Initially at open-circuit (corresponding to a higher stiffness state), the material is short-circuited (low stiffness) at peak displacement, and subsequently returned to open-circuit at equilibrium. From [16].*

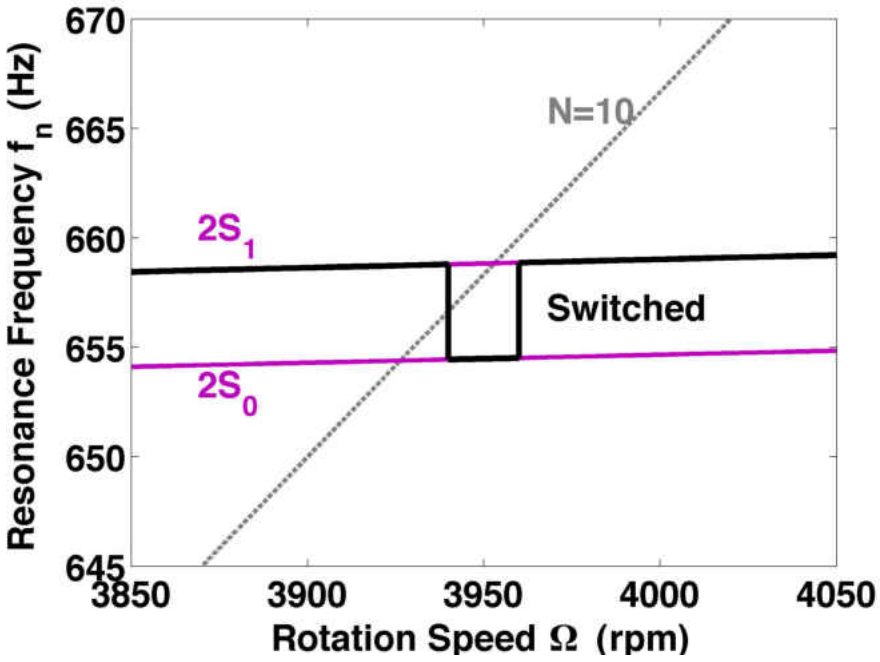

Figure 1.8: *Illustration of resonance frequency detuning concept through a zoomed view of a particular resonance crossing from Figure 1.3. The solid black line represents the resonance frequency of the structure nominally corresponding to the optimal control law.*

Resonance frequency detuning, proposed by Kauffman and Lesieutre, provides significant vibration reduction while requiring only two switches per resonance frequency crossing, thus alleviating the primary issues with many passive and semi-active approaches [8]. The purpose of this technique is to limit resonant vibration response by detuning the resonant frequency of the blade from that of the excitation through the inclusion of piezoelectric materials. Changing the electrical boundary conditions on the piezoelectric material changes its stiffness and in turn that of the entire structure and, as the resonance frequency is related to stiffness, the embedded piezoelectric material can be used to control the resonance frequency of the blade.

Figure 1.8 focuses on the intersection of the two-stripe (2S) mode resonance frequency with the $N = 10$ engine order excitation, and provides an instructive illustration of how resonance frequency

detuning works. As the resonance frequency approaches that of the excitation the structure has some nominal stiffness, corresponding to the open-circuit condition on the piezoelectric material. Just before the frequency crossing, the blade stiffness is suddenly shifted as the piezoelectric material is short-circuited. Clearly there is still an intersection as the frequency change must occur continuously, however the crossing is now nearly instantaneous and there is no appreciable increase in vibration amplitude [13]. As the rotation speed continues to increase past the frequency crossing the blade is returned to its original stiffness state, both to maintain the intended structural design and to prepare for additional stiffness changes should future frequency crossings occur.

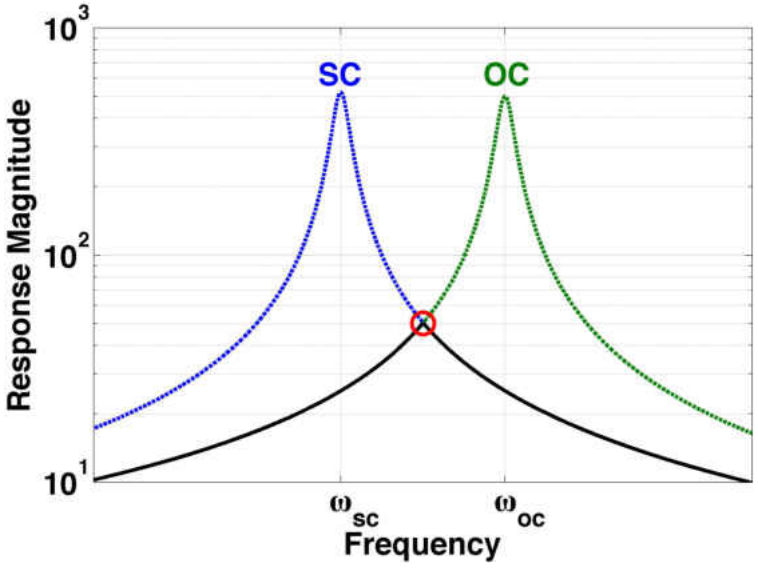

Figure 1.9: *Resonance frequency detuning concept viewed in the frequency domain. The open-circuit (OC) and short-circuit (SC) response curves are shown, as well as the optimal response, with the optimal switch circled.*

It is also constructive to view resonance frequency detuning in the frequency domain. Figure 1.9 shows the open-circuit and short-circuit frequency response curves, corresponding to the high and low stiffness states, respectively. The purpose of this approach is to minimize blade vibrations, and

it is clear that this is achieved by switching from open-circuit to short-circuit at the intersection of the two curves, as indicated by the point circled in the figure. While this frequency domain analysis inherently assumes harmonic motion, an assumption that is not valid for the frequency sweep excitations considered in this work, it provides a qualitative understanding of resonance frequency detuning and a baseline perspective with which to compare later results. Indeed, it is natural to expect that the behavior observed under swept excitations will tend toward that of harmonic excitations in the limit of slow sweeps. A further idealization made in this analysis is the use of true open- and short-circuit conditions. While these conditions provide the best vibration reduction performance, they present a problem from an energy harvesting perspective. Switching stiffness states requires a small source of power, yet true open-circuit and short-circuit conditions correspond to an infinite resistance (zero charge) and zero resistance (zero voltage) in the piezoelectric material, and thus there is no energy flow. In practice, it will be necessary to use shunts with a very high and very low resistance to approximate the true open- and short-circuit conditions, thus providing the energy source required for state-switching while essentially maintaining the ideal stiffness states. One topic of this thesis is to develop an understanding of energy harvesting capabilities under these far-from-ideal conditions which are rarely, if ever, studied in conventional energy harvesting research. Note that it should be possible to use multiple piezoelectric materials to implement this method, one for vibration control and a second tuned to harvest energy efficiently, however using a single piezoelectric material to accomplish both of these tasks reduces the size of the system and is one of the attractive feature of resonance frequency detuning.

1.4 Goals of Current Work

The goal of this research effort is to improve the understanding of piezoelectric-based energy harvesting behavior in the context of the vibration reduction technique described above, namely resonance frequency detuning. This technique reduces blade vibrations by detuning the resonant frequency of the blade from that of the excitation through a shift in stiffness, essentially caused by changing the resistance in the shunt circuit attached to the embedded piezoelectric materials [8]. Optimally the switch is from open-circuit to short-circuit, as this results in the largest shift in stiffness and, in turn, resonance frequency. Practically, however, harvesting requirements dictate that true open- and short-circuit conditions cannot be met, as there is no electrical energy flow in these cases. Implementing resonance frequency detuning therefore requires that energy be harvested very near open- and short-circuit, conditions which are far from optimal for harvesting and not studied in conventional energy harvesting research. One aspect of this research will work to develop an understanding of harvesting behavior under these non-optimal conditions – at the "margins."

As having real-time knowledge of the system's dynamics would be impractical when implementing resonance frequency detuning in the turbomachinery environment, it is desirable to use a quantity that is readily measurable on-blade, with minimal processing, as a proxy for the local vibration characteristics. One such quantity is the harvested energy. A close correlation between the harvested energy and vibration profile is anticipated as a result of the electromechanical coupling in piezoelectric materials; it is therefore proposed that the harvested energy may serve as an indicator of the optimal time to switch stiffness states in the resonance frequency detuning scheme. A metric

is developed for selecting the optimal switch in terms of a nomdimensionalized harvested energy. This metric is valid for a wide range of choices of open- and short-circuit shunt resistances, and its dependence on key system parameters is examined.

Finally, the impact of the frequency sweep rate, α, is studied. This parameter, describing the rate at which the excitation frequency is varying, does not appear in any conventional energy harvesting research, which typically focuses on steady-state or chaotic excitations. It is therefore valuable to explore this novel topic in energy harvesting; an understanding of the role of the sweep rate in energy harvesting is developed in this work.

1.5 Thesis Structure

Chapter 2 provides a review of literature which is relevant to vibration reduction in the context of resonance frequency detuning. It first discusses the nature of piezoelectricity and several important properties of piezoelectric materials, such as how they may be used to tune the stiffness of a structure. It also reviews past work in both energy harvesting and vibration reduction, to provide the background upon which this work will build.

In Chapter 3, the theoretical framework for the following analysis is developed. It is shown how the governing equations of motion arise out of a full blade dynamics model, explaining and justifying any assumptions which were made to arrive at the final form of these equations. The model is subsequently applied to the case of steady-state vibrations, deriving expressions for the relationship between the power output of the harvesting system and the effective structural stiffness

arising from the integration of piezoelectric materials. The chapter then discusses how a solution may be obtained for transient vibrations through direct time integration, and, as this method turns out to be computationally expensive, an analytic solution is then pursued.

Chapter 4 then uses this information to analyze the behavior that is of interest here. First the power output of the harvesting system is examined in terms of the physical system parameters, namely the coupling coefficient, excitation frequency, and modal damping ratio. The problem is then reparametrized in terms of an effective structural stiffness, as is laid out in Chapter 3, a process which indicates behavior that may surprise many conventional energy harvesting researchers. Proceeding to the case of transient vibrations, the relationship between harvested energy and blade vibrations is examined. In particular, the energy that has been harvested at the time of switching between open- and short-circuit conditions is correlated with the peak vibration response of the system, with the intent that the harvested energy may be used to trigger the optimal switch in stiffness states. This chapter concludes by studying the effect of the frequency sweep rate on both the harvested energy and vibration reduction. This is particularly important for resonance frequency detuning, as it is a vibration reduction technique for systems with changing excitation frequencies, and it is this sweep rate that describes the rate at which the frequency is changing.

Finally, Chapter 5 provides a review of the key findings of this research and discusses their implications for resonance frequency detuning. The thesis concludes by presenting remaining questions and how one may proceed in continuing this research effort.

CHAPTER 2
REVIEW OF PREVIOUS WORK

The use of piezoelectric materials in intelligent systems has received significant attention over the last several decades, with a number of applications studied. Despite the wide range of applications, the principles applied in much of this work are the same, and it is important to understand the breadth of past work and its implications, and thus build upon that foundation. Foremost, one must understand the nature of piezoelectric materials and how they make this work possible.

2.1 Piezoelectricity

Discovered by the physicists Jacques and Pierre Curie in 1880, piezoelectric materials have an inherent coupling between their mechanical and electrical properties [17]. In what is known as the direct piezoelectric effect, application of a mechanical stress to a piezoelectric material generates of an electric field within that material. Conversely, the application of an electric field mechanically deforms the material. The latter phenomenon, the indirect piezoelectric effect, was postulated by Gabriel Lippmann after in-depth mathematical investigation of the thermo-mechanical behavior of piezoelectric materials [17]. The existence of this indirect effect was then demonstrated in practice

by the Curie brothers, who found that the application of a electric field does indeed produce a mechanical deformation within the material [17].

2.1.1 Physical Origin

To understand the physical origin of both the direct and indirect piezoelectric effect, one must consider the crystal lattice molecular structure of a material. Present in many classes of crystals, piezoelectricity always arises in noncentrosymmetric crystals – those that lack a center of symmetry [18]. As a characteristic example, Figure 2.1 shows the structure of a unit cell of calcium titonate (CaTiO3). The unit cell has a non-zero net charge due to the titanium ion, and this ion's off center location effectively creates an electric dipole. On a macroscopic scale, these dipoles are naturally oriented randomly, resulting in no net polarization. Through a poling process, depicted in Figure 2.2, the many electric dipole moments in the material can be aligned, typically through the application of a very strong electric field – a process similar to the magnetization of ferromagnetic materials. Upon removing the material from the polarizing field there is a remnant polarization, which is responsible for the macroscopic piezoelectric properties of a material [18]. Through the application of a mechanical pressure, the structure begins to deform, causing a shift in the orientation of the dipoles. As a result, a net electrical charge displacement is established within the material, thus constituting an electric field. This process is known as the direct piezoelectric effect. In the case of the indirect piezoelectric effect, the application of an electric field forces a reorientation of the electric dipoles, thus displacing the ions within the material and causing the structure to deform.

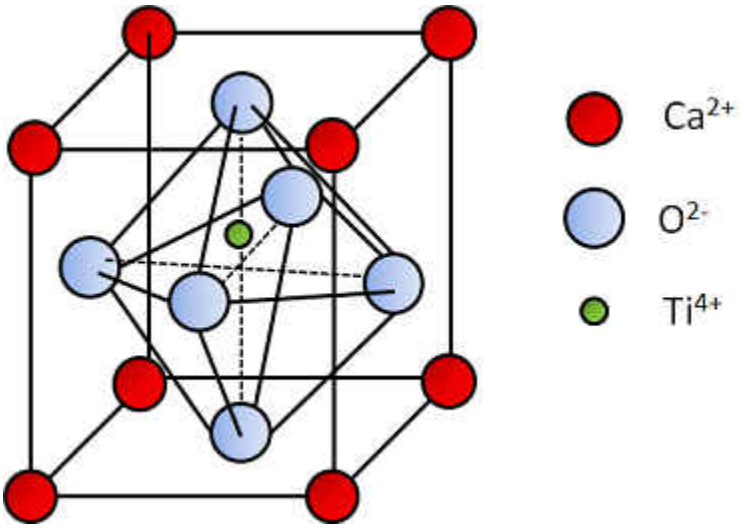

Figure 2.1: *Structure of a unit cell of calcium titonate (CaTiO3). From [18].*

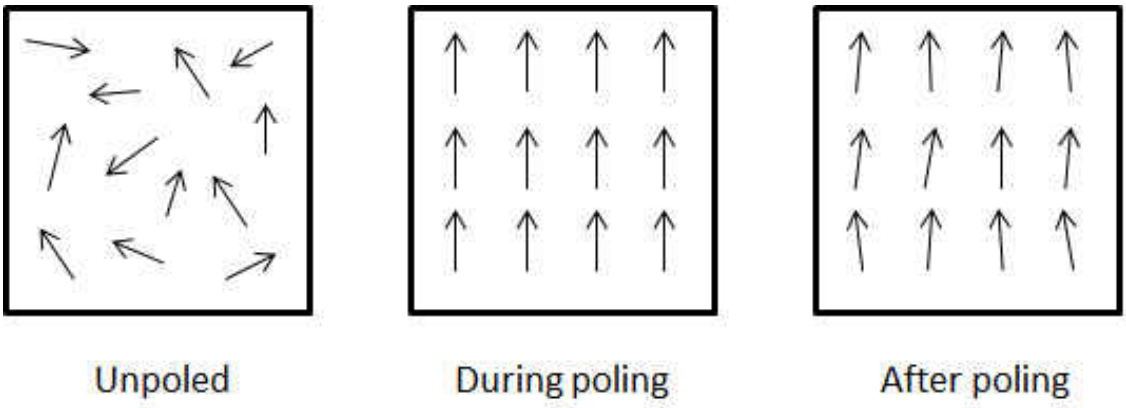

Figure 2.2: *Aligning of electric dipole moments before, during, and after the poling process. From [18].*

A simple example is provided by Figure 2.3 to orient the reader toward this behavior. The poling axis is indicated as positive down. Application of an electric field with the same polarity as that of the material causes the material to expand along that axis. Similarly, application of an electric field with the opposite polarity results in a contraction along that axis. Generalizing, we see that application of a AC voltage along the poling direction results in a mechanical vibration with the same period as that of the excitation. In a similar manner, a piezoelectric material with forced mechanical vibrations will produce an internal AC voltage as mechanical pressure is periodically applied and relieved. This behavior forms the basis for piezoelectric-based vibration energy harvesting, as piezoelectric materials can be embedded within structures with externally forced vibrations, thus generating a voltage within the material that can be used to power a device or stored for later use.

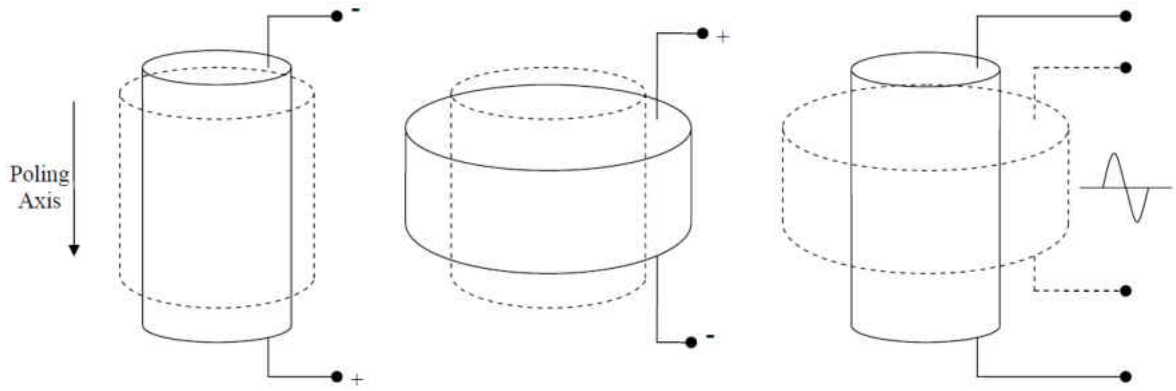

Figure 2.3: *Depiction of the indirect piezoelectric effect. From [19].*

2.1.2 Constitutive Relations

The electromechanical coupling exhibited by piezoelectric materials can be expressed through several constitutive forms, each having its own coupling coefficients. The linear stress-field form, for example, takes the form

$$\begin{Bmatrix} T \\ E \end{Bmatrix} = \begin{bmatrix} c^D & -h^t \\ -h & (\varepsilon^S)^{-1} \end{bmatrix} \begin{Bmatrix} S \\ D \end{Bmatrix}, \tag{2.1}$$

relating S and D, the strain and electric displacement vectors, to (T) and (E), the stress and electric field vectors, through the elastic coefficients (c) , the electromechanical coupling coefficients (h), and the permittivity (ε) [20]. Here t is the transpose operator, while the superscripts S and D denote that a quantity is to be taken at constant strain and constant electric displacement, respectively. Note that the coefficients in the coupling matrix can be found under other boundary conditions as well. The matrix of elastic coefficients at constant electric field, for example, can be found by setting the electric field, E, equal to zero in Equation (2.1):

$$\left[c^E\right] = \left[c^D\right] - \left[h^t\right]\left[\varepsilon^S\right][e] \tag{2.2}$$

2.1.3 Electromechanical Coupling Coefficient

The coupled electrical and mechanical behavior of piezoelectric materials is more intuitively expressed via the electromechanical coupling coefficient, k [20]. This coefficient provides a direct

measure of a material's ability to convert energy between mechanical and electrical forms. When squared, as it more commonly appears in practice, this coefficient is defined as the ratio of the energy converted to that imposed on the structure. Such a coefficient exists for each coupling mode, where only a single stress or strain and a single electric field or displacement component is non-zero, and for each vibrational mode, as the coupling coefficient is dependent on the excitation frequency. Additionally, this coupling coefficient can be defined for a device with embedded piezoelectric materials, potentially leading to higher coupling coefficients than for the material alone. In terms of the various coefficients appearing in the constitutive relations described in the previous section, the coupling coefficient can be expressed mechanically as the shift between the open-circuit and short-circuit stiffness,

$$k^2 \equiv \frac{c^D - c^E}{c^D}, \tag{2.3}$$

and electrically as the shift between open-circuit and short-circuit permittivity,

$$k^2 \equiv \frac{\varepsilon^T - \varepsilon^S}{\varepsilon^T}. \tag{2.4}$$

Using, for example, the scalar form of the result in Equation (2.2), this becomes

$$k^2 \equiv \frac{h^2 \varepsilon^S}{c^E + h^2 \varepsilon^S}. \tag{2.5}$$

Another, perhaps more useful, expression for the coupling coefficient is found by writing Equation (2.3) in terms of the open-circuit and short-circuit resonance frequencies:

$$k^2 = \frac{\omega_{oc}^2 - \omega_{sc}^2}{\omega_{oc}^2}. \tag{2.6}$$

A structure's coupling coefficient can therefore be determined experimentally by simply measuring the natural frequency at open-circuit and short-circuit boundary conditions.

2.1.4 Stiffness Control

The integration of piezoelectric materials in a structure allows for significant tailoring of structural properties, due to the coupling between electrical and mechanical behavior. By comparing the equations of motion governing the behavior of a simple energy harvesting device with those of the canonical second order single-degree-of-freedom dynamic system, an expression for the effective stiffness of a structure can be established [21]. This effective stiffness varies strongly with the electrical impedance, with the magnitude of the shift in stiffness states from open- to short-circuit dictated by the coupling coefficient, as can be seen in Figure 2.4.

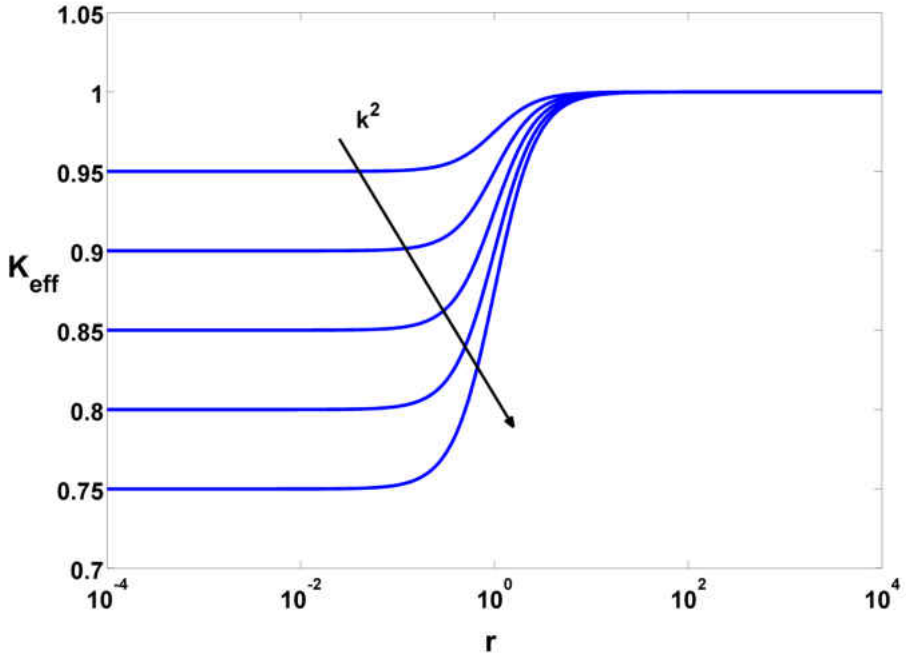

Figure 2.4: *Variation of the effective structural stiffness with shunt circuit resistance, for coupling coefficient* $k^2 = 5\%, 10\%, 15\%, 20\%, 25\%$.

$$K_{\text{eff}} = 1 - \frac{k^2}{1 + \Omega^2 r^2} \tag{2.7}$$

Therefore, by switching between two resistive shunts near the open- and short-circuit conditions, the stiffness of a structure can be shifted, in the process detuning the resonance frequency, as desired. Note that the derivation of Equation (2.7) relies on harmonic analysis, and Ω and r are the dimensionless frequency of excitation and shunt circuit resistance, respectively.

2.1.5 Temperature Limitations

It is important to note that this research effort is currently intended for the turbofan and cold side of the compressor, due in part to the temperature limitations of piezoelectric materials. At a material's Curie temperature, the crystal structure breaks down and a phase shift occurs, resulting in a crystal structure that does not exhibit piezoelectricity. This temperature limit of the piezoelectric properties can be seen in Figure 2.5; it is apparent that most materials lose their piezoelectric coupling in the range of 200-350°C. [22] There are, however, efforts to develop high temperature piezoelectric materials, and it may be that this resonance frequency detuning approach can be extended further into the engine in the future.

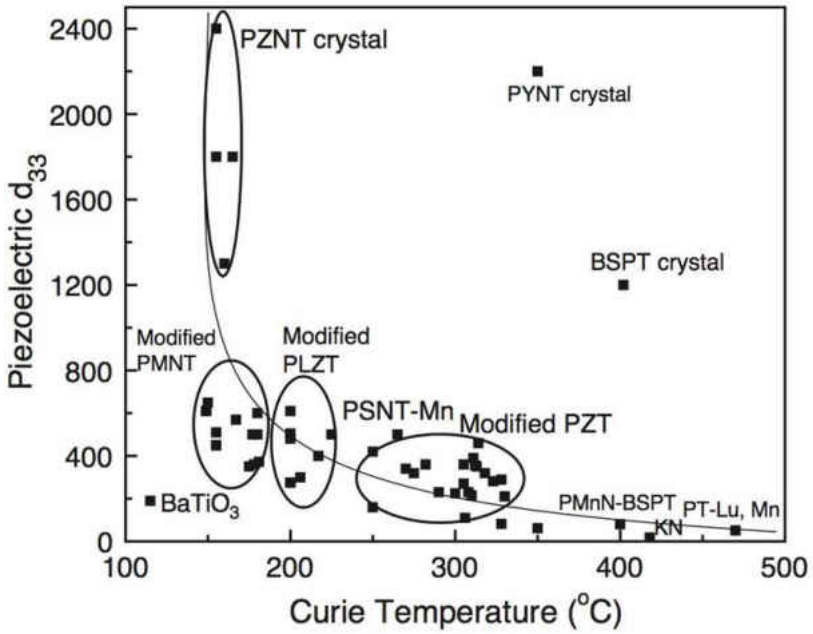

Figure 2.5: *Degradation of piezoelectric effect with increasing temperature. Note that this is not a theoretical limit, but simply the state-of-the-art for piezoelectric materials at the time of publication. From [22].*

2.2 Energy Harvesting

There has been a significant effort to improve the performance piezoelectric-based vibrational energy harvesting devices over the past few decades, with a variety of different approaches to the problem being taken. Some researchers have worked to develop more effective piezoelectric materials by either achieving higher coupling coefficients, reducing susceptibility to crack development, or improving upon current temperature limitations. Taking another approach, many seek to understand the role of key physical and geometric parameters so their optimal values may be chosen for a particular system, thus optimizing the performance of the energy harvesting system. Finally, advanced harvesting circuits have been developed by adding switching devices and inductors in various configurations; the resulting voltage inversion often leads to a significant improvement in performance.

Sodano et al. tested three common piezoelectric material configurations: a bimorph Quick Pack actuator (QP), the piezoceramic material lead-zirconate-titanate (PZT), and a macro-fiber composite (MFC) [23]. Each was subjected to several excitation conditions – resonant excitations, random vibrations, and a $0-500\ Hz$ chirp; it was found that in each case PZT exhibited a more efficient energy conversion that the other configurations. Unfortunately, PZT is very brittle and thus susceptible to fatigue cracking when subjected to high frequency excitations, limiting their effectiveness for turbomachinery vibration reduction applications where high frequency excitations are common. Attempting to alleviate this drawback, Sato et al. developed composite materials with

embedded PZT fibers [2, 24]. PZT fibers, which can be produced via an electrospinning process, exhibit a much lower bending stiffness, and are thus less susceptible to fatigue cracking [25].

Taking an alternative approach to improving the efficiency of piezoelectric energy harvesting devices, some researchers have worked to optimize the physical parameters of the system, with a particular focus on the dimensions of the piezoelectric material and the tip mass [26, 27]. A tip mass is often included to reduce the resonance frequency of the first vibration mode – it is well known that the power output of harvesting systems is increased at lower frequencies; increasing the proof mass thus results in improved performance. [28]. It was found that matching the mechanical impedance of the structure – dependent on the geometry of the device and Young's modulus – to that of the load led to a substantial improvement in the device's effectiveness at converting energy. Note that this concept – impedance matching – has an analog in several other disciplines – matching the electrical impedance in electrical engineering, matching the index of refraction at an interface in optics, and matching heat transfer coefficients at an interface, each of which increases the efficiency of energy transfer.

Renno et al. studied the effect of the damping ratio on power optimality, setting up a nonlinear optimization problem through a method similar to the method of Lagrange multipliers. They found that, contrary to claims made in previous literature, the power output of the harvesting system begins to decrease as the coupling coefficient increases past some optimal value [29]. Additionally, they found that the optimal power output bifurcates as the damping ratio drops below what is termed the bifurcation damping ratio – that is, below this value of the damping ratio there are two maxima in

the power output at two distinct frequencies – the resonance and antiresonance. This trend toward a bimodal distribution as the damping ratio decreases can be seen in Figure 2.6.

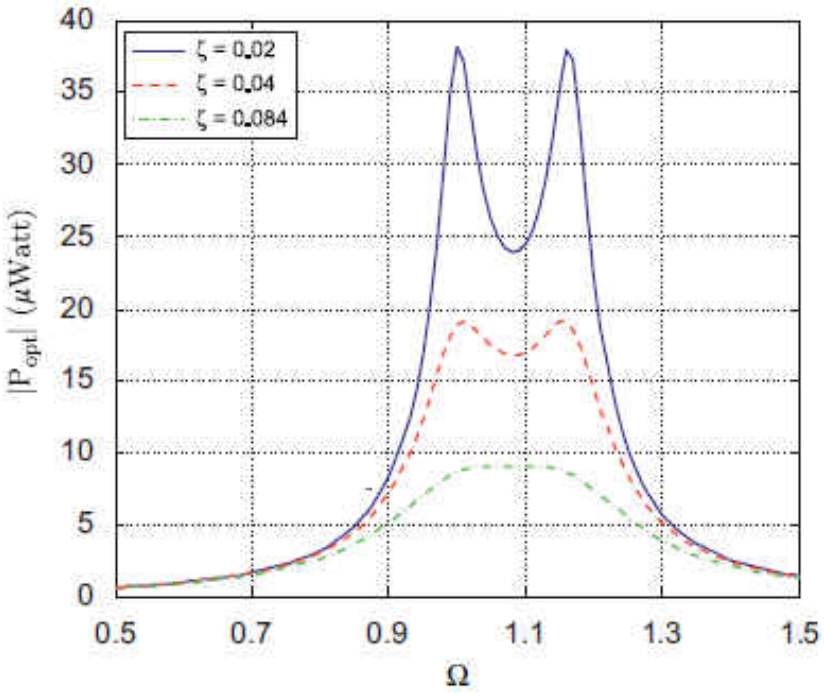

Figure 2.6: *Magnitude of harvested power as a function the nondimensional frequency, Ω, at different damping ratios, ζ. From [29].*

Taking yet another approach to improving the performance of piezoelectric energy harvesting devices, Badel et al. proposed several advanced harvesting circuits, termed synchronized switch harvesting (SSH) and subsequently synchronized switch harvesting on an inductor (SSHI) [30, 31]. These methods improve upon standard energy harvesting configurations by adding a switching device in parallel with the circuit; triggering the switch at peak displacement results in a voltage inversion which increases the voltage amplitude on the piezoelectric material, thus improving the performance of the device. Indeed, the power output was observed to increase by as much as 400% as compared with a standard resistive shunt. In this analysis the authors make several assumptions

which must be relaxed in portions of this work: they assume steady-state harmonic forcing, clearly not valid for a system with frequency sweep excitations, and they assume the system is driven near resonance, again, not valid in an approach where excitation conditions are changing time and the precise goal is to avoid resonance conditions. Further, in assuming the system is driven near resonance they make the assertion that the applied forced and velocity are in phase – a valid assumption for undamped (or very lightly damped), single degree of freedom systems. Shu and Lien, however, have challenged this assumption [3]. In their analysis, Shu and Lien found that in-phase assumption is only valid for $]frack^2\zeta \ll 1$, even when operating near resonance.

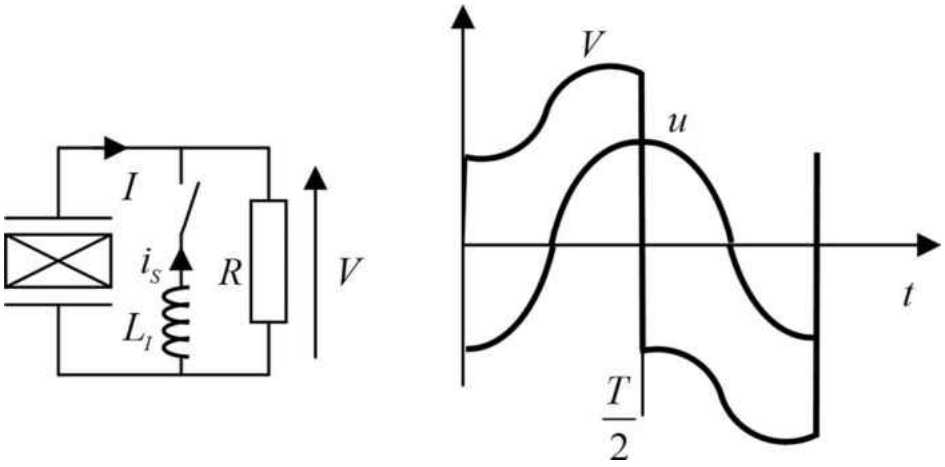

Figure 2.7: *Circuit diagram and typical displacement and voltage waveforms for a synchronized switch harvesting device. This particular setup includes an inductor to further enhance performance. From [30].*

2.3 Vibration Control

In a manner analogous to energy harvesting devices, piezoelectric energy conversion is commonly used for vibration control. The energy can be stored or simply dissipated, for example though a

resistor, effectively acting as a source of damping as mechanical energy is removed through the harvesting system.

An early example of a passive vibration control system using piezoelectric materials was presented by Hagood and von Flotow [14]. They investigated shunting the piezoelectric material with both a lone resistor and a combined resistive-inductive circuit, finding that resistive shunting shows behavior similar to that of viscoelastic materials, while shunting on a resistor and inductor produces an electrical resonance which may be tuned to structural resonances to optimize performance. Lesieutre et al. studied the damping associated with a piezoelectric-based energy harvesting system under harmonic excitation conditions, finding that for their system the effective modal loss factor depended on the electromechanical coupling coefficient as well as the voltage ratio of the bridge rectifier [32].

Clark developed a semi-active vibration control system, taking advantage of the stiffness change associated with changing the electrical boundary conditions on piezoelectric materials [16]. The circuit is shorted at peak mechanical displacement (peak strain energy) and opened at peak kinetic energy. It was found that, while a finely-tuned passive system may provide more effective vibration reduction at resonance, the state-switching method is more effective away from resonance, requiring no tuning and showing less sensitivity to changes in system parameters. Similarly, Richard et al. proposed a technique called synchronized switch damping [33]. In this method, the circuit is periodically switched between open- and short-circuit; however, the circuit is only shorted long enough to dissipate the energy before returning to open-circuit. By introducing a phase lag between the beam deflection and shunting frequency, the resulting damping was found to be twice as effective

as a purely resistive passive shunt, while also being broadband. This approach was then enhanced by adding an inductor to the shunt, resulting in a charge inversion that further improved performance with proper tuning of the switching frequency [34].

While the vibration control approaches discussed have been shown to be very effective in many applications, there are several factors that hinder their use in turbomachinery applications. In the case of passive techniques, the system must be well tuned to the resonance of each targeted mode of vibration to be effective. In turbomachinery, where a large number of modes with varying excitation frequencies must be targeted, the scale of the vibration control system would quickly become too large as additional branches are added to the circuit for each mode. Semi-active techniques, while possessing the broadband damping capabilities needed for turbomachinery applications, have potentially prohibitive switching requirements. Though very effective in low-frequency applications, the need to switch states as many as four times per vibration cycle requires real-time detailed knowledge of the structure's motion in addition to an external power supply for the switching device, each presenting problems for implementation in the frame of a rotating turbomachinery blade. As a result a new vibration reduction approach, resonance frequency detuning, was proposed by Kauffman and Lesieutre specifically for turbomachinery blades with transient excitations [35].

Kauffman and Lesieutre then studied the performance of piezoelectric-based vibration damping and control techniques in structures subjected to frequency-sweep excitations [36], and considered their feasibility for implementation in turbomachinery. A vibration control approach for turbomachinery blades would necessarily target multiple modes; it is then clear that passive approaches, which must be finely tuned to the excitation condition of the targeted mode, are less practical.

Kauffman and Lesieutre determined that state switching, synchronized switched damping, and resonance frequency detuning are the most practical for this application, and that, while all three methods are effective, synchronized switched damping achieves the greatest reduction in vibration. Despite other approaches delivering slightly better performance, resonance frequency detuning appears to be preferable for turbomachinery as the significantly reduced switching requirements necessitate less power and less hardware than other semi-active approaches.

CHAPTER 3
MODEL DEVELOPMENT

To pursue the desired analysis, a dynamics model for the blade and integrated piezoelectric materials is required. The following section discusses how this model arises and, as even this low-order model is unnecessarily complex for the analysis to follow, a number of simplifications and nondimensionalizations are then proposed. The resulting set of nondimensional equations of motion are then used to study both steady-state and transient energy harvesting behavior in the context of resonance frequency detuning. An expression relating the effective structural stiffness to the key parameters of the energy harvesting system is derived, and subsequently the power output of the harvesting system is expressed in terms of this effective stiffness. Time-integration of the equations of motion is then discussed for a treatment of transient vibrations, followed by an analytic solution that is pursued in the interest of reducing computation time.

3.1 Discretized Equations of Motion

To conduct a transient analysis of the system, we must proceed in the time domain. Here we begin with a low-order dynamics model of the turbomachinery blade and incorporated piezoelectric

materials, which was previously developed using the assumed modes method: [37]

$$\begin{bmatrix} M_m & 0 \\ 0 & 0 \end{bmatrix} \begin{Bmatrix} \ddot{w}_m \\ \ddot{w}_e \end{Bmatrix} + \begin{bmatrix} C_m & 0 \\ 0 & 0 \end{bmatrix} \begin{Bmatrix} \dot{w}_m \\ \dot{w}_e \end{Bmatrix} + \begin{bmatrix} K_m + \Omega^2 K_g & -K_c^t \\ -K_c & K_e^{-1} \end{bmatrix} \begin{Bmatrix} w_m \\ w_e \end{Bmatrix} = \begin{Bmatrix} F_m \\ F_e \end{Bmatrix}. \tag{3.1}$$

Here w_m and w_e, arising as the weights of the assumed mode shapes, become the generalized mechanical and electrical coordinates, respectively, while M, C, K, and F are the various mass, damping, stiffness, and forcing terms – see the appendix for full details. For an initial analysis of the problem it is desirable to simplify the problem further, as a large number of parameters appear in Equation (3.1). To this end several simplifying assumptions are made. We first assume an idealized swept sinusoidal excitation of constant amplitude to represent the aerodynamic forces resulting from rotor-stator interactions. Further, the geometric stiffness term, $\Omega^2 K_g$, is assumed constant and incorporated in the mechanical stiffness. This assumption is justified by assuming a restricted range of operating frequencies and thus that the stiffening (alternatively, softening) due to this term is time independent. Finally, we assume a single degree of freedom for the mechanical and electrical coordinates and, after nondimensionalization, arrive at the simplified equations of motion:

$$\begin{aligned} u'' + 2\zeta u' + u - q &= \sin\phi(\tau) \\ -k^2 u + q &= U. \end{aligned} \tag{3.2}$$

Here ζ is the modal damping ratio, while u, q, and U are the nondimensional displacement, charge displacement, and voltage, respectively. Primed quantities indicate differentiation with respect to the nondimensional time, τ. A full derivation is available in the appendix. The time-varying phase

of excitation, $\phi(\tau)$, is given by

$$\phi(\tau) = \frac{\alpha}{2}\tau^2 + \alpha_0\tau + \psi. \tag{3.3}$$

Without a loss of generality, the constant part of the phase, ψ, is commonly taken to be zero. In addition, we consider sweeps of zero initial frequency, such that $\alpha_0 = 0$. The instantaneous frequency, or scaled time, is then given by $\omega = \alpha t$, where α is the frequency sweep rate, a quantity of prime interest here.

3.2 Steady-State Analysis

In steady-state applications, the equations of motion can be simplified one step further, with the phase of excitation reduced to $\phi(\tau) = \Omega\tau$, where Ω is the excitation frequency scaled by the open-circuit natural frequency of the system. Equation (3.2) then becomes

$$\begin{aligned} u'' + 2\zeta u' + u - q &= e^{i\Omega\tau} \\ -k^2 u + q &= U. \end{aligned} \tag{3.4}$$

3.2.1 Resistive Shunt

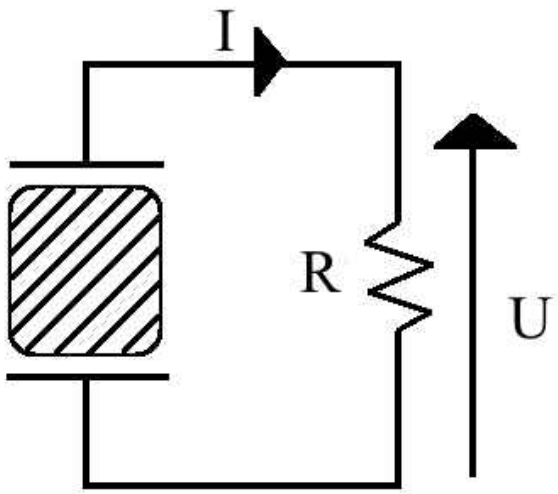

Figure 3.1: *AC Resistive Shunt.*

Though a number of advanced harvesting circuits have been developed, there is no clear benifit to their use in this application as these circuits are generally designed to increase power output, which is of little concern here. Indeed, due to size limitations for a practical implementation of resonance frequency detuning it is desirable limit any nonessential additional hardware. As a result only resistive shunts, as in Figure 3.1, will be considered hereFigure 3.1. The dimensionless voltage can then be determined via Ohm's law:

$$U = IR = -\dot{q}r. \tag{3.5}$$

Working toward an expression for the piezoelectric charge displacement, q, Equation (3.5) can be used to replace U in the second equation in Equation (3.4):

$$-k^2u+q=-\dot{q}r=-i\Omega qr, \tag{3.6}$$

Now, moving to the frequency domain, this becomes

$$\tilde{q}=\frac{k^2}{1+i\Omega r}\tilde{u}, \tag{3.7}$$

where i is the imaginary unit and tildes are used to indicate complex quantities. Substituting this expression for the charge displacement in Equation (3.5), the (complex) voltage on the piezoelectric patch is then

$$\tilde{U}=-i\Omega\tilde{q}r=\frac{-k^2r}{1+i\Omega r}i\Omega\tilde{u}. \tag{3.8}$$

Equation (3.4) is then rearranged to yield an expression for $\tilde{u}$:

$$\tilde{u}=\frac{1}{-\Omega^2+2i\Omega\zeta+1-\frac{k^2}{1+i\Omega r}} \tag{3.9}$$

Taking the magnitude of $\tilde{u}$, the mechanical displacement is now known in terms of the key system parameters:

$$u = |\tilde{u}| = \sqrt{|\tilde{u}\tilde{u}^*|} = \Big[\Omega^4 - 2\Omega^2 + 4\zeta^2\Omega^2 + 1 + 2\frac{k^2\Omega^2}{1+\Omega^2 r^2} + 4\frac{\zeta k^2\Omega^2 r}{1+\Omega^2 r^2} - 2\frac{k^2}{1+\Omega^2 r^2} + \frac{k^4}{(1+\Omega^2 r^2)^2} + \frac{k^4\Omega^2 r^2}{(1+\Omega^2 r^2)^2}\Big]^{-1/2}$$
$$= \left[\Omega^4 - 2\Omega^2 + 4\zeta^2\Omega^2 + 1 + \frac{k^2}{1+\Omega^2 r^2}\left(k^2 + 2\Omega^2 + 4\zeta\Omega^2 r - 2\right)\right]^{-1/2} \quad (3.10)$$

To this point the only assumptions that have been made are those which led to the dimensionless equations of motion in Equation (3.4); namely, that harvesting occurs over a limited range of rotation speeds, that the modes are well enough separated that a single degree of freedom can be considered, and that the excitation is a constant magnitude sinusoid with a changing frequency. Many energy harvesting researchers, however, often make the additional assumption of operating very near resonance (that is, $\Omega \approx 1$) [30]. This assumption leads to a simplified expression:

$$u = \left[2\zeta + \frac{k^2 r}{1+r^2}\right]^{-1}. \quad (3.11)$$

Guyomar at al. for example, arrive at this expression (though in terms of dimensional quantities and using different notation) by making the assumption that the forcing and velocity of the beam deflection are in phase at resonance, which appears to be a good assumption for low coupling [30].

To understand how they arrive at this expression, start by rearranging Equation (3.9):

$$\tilde{u} = \left[\Omega^2 + 2i\Omega\zeta + 1 + \frac{k^2 i\Omega r}{1+\Omega^2 r^2} - \frac{k^2 r^2 \Omega^2}{1+\Omega^2 r^2}\right]^{-1} \tag{3.12}$$

The assumption that the forcing and velocity of the beam deflection are in phase at resonance mathematically amounts to setting the real components of this expression equal to zero:

$$\tilde{u} = \left[2i\Omega\zeta + \frac{k^2 i\Omega r}{1+\Omega^2 r^2}\right]^{-1} \tag{3.13}$$

Upon setting $\Omega = 1$ and taking the magnitude of this expression, Equation (3.11) is recovered. Interestingly, the same expression is not found by simply setting $\Omega = 1$ in Equation (3.10) and using the assumption of low coupling:

$$u = \left[1 - 2 + 4\zeta^2 + 1 + \frac{k^2}{1+r^2}\left(k^2 + 2 + 4\zeta r - 2\right)\right]^{-1/2} \tag{3.14}$$

$$= \left[4\zeta^2 + \frac{k^2}{1+r^2}\left(k^2 + 4\zeta r\right)\right]^{-1/2} \tag{3.15}$$

$$= \left[4\zeta^2 + \frac{k^4}{1+r^2} + \frac{4\zeta k^2 r}{1+r^2}\right]^{-1/2} \tag{3.16}$$

$$\approx \left[4\zeta^2 + \frac{4\zeta k^2 r}{1+r^2}\right]^{-1/2} \tag{3.17}$$

$$\approx \left[2\zeta + \frac{k^2 r}{1+r^2}\right]^{-1}. \tag{3.18}$$

The last step is only made clear by working backward: after taking the square of the last line, using the assumption of low coupling to set higher order terms (k^4) to zero, and taking the square root of

the result, the previous expression can be recovered. However, the purpose of this work is precisely to develop an understanding of energy harvesting behavior far from optimal conditions, and this assumption is not valid. The general expression given by Equation (3.10) will therefore be used in further analysis.

Finally, the power dissipated in the resistive shunt is:

$$P = \frac{\tilde{U}\tilde{U}^*}{2r} = \frac{k^4\Omega^2 r}{1+\Omega^2 r^2}\frac{u^2}{2} \tag{3.19}$$

$$= \frac{k^4\Omega^2 r}{2\left(1+\Omega^2 r^2\right)}\left[\Omega^4 - 2\Omega^2 + 4\zeta^2\Omega^2 + 1 + \frac{k^2}{1+\Omega^2 r^2}\left(k^2 + 2\Omega^2 + 4\zeta\Omega^2 r - 2\right)\right]. \tag{3.20}$$

3.2.2 Effective Stiffness

Of interest in this work is understanding how changes in the stiffness near the open- and short-circuit conditions affect the power output of the harvesting system. As such, it is useful to re-parametrize the system in terms of an effective structural stiffness involving the key parameters of the harvesting system; this is pursued here [14]. Equation (3.4), when expressed in the frequency domain, becomes

$$\begin{aligned} -\Omega^2\tilde{u} + 2\zeta i\Omega\tilde{u} + \tilde{u} - \tilde{q} &= \tilde{f} \\ -k^2\tilde{u} + \tilde{q} &= \tilde{U}. \end{aligned} \tag{3.21}$$

As in the previous section, the second equation is solved for $\tilde{q}$, while $\tilde{U}$ is replaced by Equation (3.8), yielding:

$$\tilde{q} = k^2\tilde{u} - \frac{k^2 r}{1+i\Omega r} i\Omega\tilde{u}. \tag{3.22}$$

Upon substituting this expression in the first line of Equation (3.21), the coupled equations of motion

$$-\Omega^2\tilde{u} + 2\zeta i\Omega\tilde{u} + \tilde{u} - k^2\tilde{u} + \frac{k^2 r}{1+i\Omega r} i\Omega\tilde{u} = \tilde{f} \tag{3.23}$$

$$-\Omega^2\tilde{u} + 2\zeta i\Omega\tilde{u} + \tilde{u} - k^2\tilde{u} + \frac{k^2 i\Omega r}{1+\Omega^2 r^2} - \frac{k^2 r^2\Omega^2}{1+\Omega^2 r^2} = \tilde{f}. \tag{3.24}$$

In the second line the complex denominator has been rationalized to facilitate the next step. After regrouping terms appropriately,

$$-\Omega^2\tilde{u} + \left(2\zeta + \frac{k^2 r}{1+\Omega^2 r^2}\right) i\Omega\tilde{u} + \left(1 - k^2 + k^2\frac{\Omega^2 r^2}{1+\Omega^2 r^2}\right)\tilde{u} = \tilde{f}. \tag{3.25}$$

By comparison with the canonical second order, single degree-of-freedom equation of motion as expressed in the frequency domain, it is now apparent that an effective damping term is present (note the similarity to Equation (3.11) – they are identical after setting $\Omega = 1$!) ,

$$\zeta_{\text{eff}} = \zeta + \frac{k^2 r}{2(1+\Omega^2 r^2)} \tag{3.26}$$

$$= \frac{u^{-1}}{2}\bigg|_{(3.11),\Omega=1} \tag{3.27}$$

and an effective stiffness term,

$$\begin{aligned} K_{\text{eff}} &= 1 - k^2 + k^2 \frac{\Omega^2 r^2}{1 + \Omega^2 r^2} \\ &= 1 - \frac{k^2}{1 + \Omega^2 r^2}. \end{aligned} \tag{3.28}$$

The latter quantity is presently of greater interest. At the short-circuit ($r = 0$) and open-circuit ($r \to \infty$) conditions, the effective stiffness takes on the limiting values:

$$K_{\text{eff,sc}} = 1 - k^2 \qquad\qquad K_{\text{eff,oc}} = 1. \tag{3.29}$$

It is useful to study how a small shift in effective stiffness affects the power output near open- and short-circuit conditions, as it is by operating near these conditions that resonance frequency detuning is most effective. In light of this, the dependance of power output on this effective stiffness is now derived. Rewriting Equation (3.25) in terms of the newly defined effective damping and effective stiffness gives the equation

$$-\Omega^2 \tilde{u} + i2\zeta_{\text{eff}} \Omega \tilde{u} + K_{\text{eff}} \tilde{u} = \tilde{f}. \tag{3.30}$$

An expression for the mechanical displacement can then be found by solving the above equation for $\tilde{u}$ and taking its magnitude:

$$u = |\tilde{u}\tilde{u}^*| = \left[\Omega^4 - 2\Omega^2 K_{\text{eff}} + 4\Omega^2 \zeta_{\text{eff}}^2 + K_{\text{eff}}^2\right]^{-1/2}. \tag{3.31}$$

Substituting this expression into Equation (3.19), the harvested power in terms of the effective stiffness is

$$P = \frac{k^4 \Omega^2 r}{2(1+\Omega^2 r^2)} \left[\Omega^4 - 2\Omega^2 K_{\text{eff}} + 4\Omega^2 \zeta_{\text{eff}}^2 + K_{\text{eff}}^2 \right]. \tag{3.32}$$

3.3 Transient Analysis

For transient analysis of the system dynamics, Equation (3.2) is integrated via a fourth-order Runge-Kutta numerical integration scheme, in particular MATLAB's built-in ode45 function. The piezoelectric voltage and power output can be calculated from the numerical solution as:

$$U = -k^2 u + q \tag{3.33}$$

and

$$P = \frac{U^2}{r}. \tag{3.34}$$

To orient the reader toward the behavior of a system with transient swept excitations, the characteristic response and power output of the system are shown in Figure 3.2. Note in particular that the resonant response is delayed compared to that of a system under harmonic excitations, and that there is an oscillation in the envelope after passing through resonance. Examining these figures, several possible methods of defining optimal resonance frequency detuning present themselves: one could minimize the overall peak response magnitude, the time it takes for the subsequent oscillations in the envelope to drop below a threshold value, or possibly a time-averaged response over the period

of interest. The first metric is chosen here, both for its simplicity and intuitive nature – the goal of resonance frequency detuning is to reduce resonant response, thus minimizing the peak response seems natural.

3.3.1 Analytic Solution

Direct time-integration of the equations of motion can become very expensive computationally, particularly for sweep rates $\alpha < 10^{-4}$ [38]. As a result, it would be advantageous to derive an analytic solution, thus reducing the computational resources needed in future analysis. Markert and Siedler presented an analytic solution for the response of a single-degree-of-freedom system driven through resonance under constant angular acceleration [39]; an analogous solution for multi-degree-of-freedom systems is sought here. In deriving the desired expression it is necessary to use the matrix exponential. First the system is written in first-order form,

$$[A]\{z'\} + [B]\{z\} = \{f\}, \tag{3.35}$$

where

$$\{z\} = \begin{Bmatrix} u' \\ u \\ q \end{Bmatrix} \quad [A] = \begin{bmatrix} 1 & 0 & 0 \\ 0 & 1 & 0 \\ 0 & 0 & r \end{bmatrix} \quad [B] = \begin{bmatrix} 2\zeta & 1 & -1 \\ -1 & 0 & 0 \\ 0 & -k^2 & 1 \end{bmatrix} \quad \{f\} = \begin{Bmatrix} \sin\phi(t) \\ 0 \\ 0 \end{Bmatrix}. \tag{3.36}$$

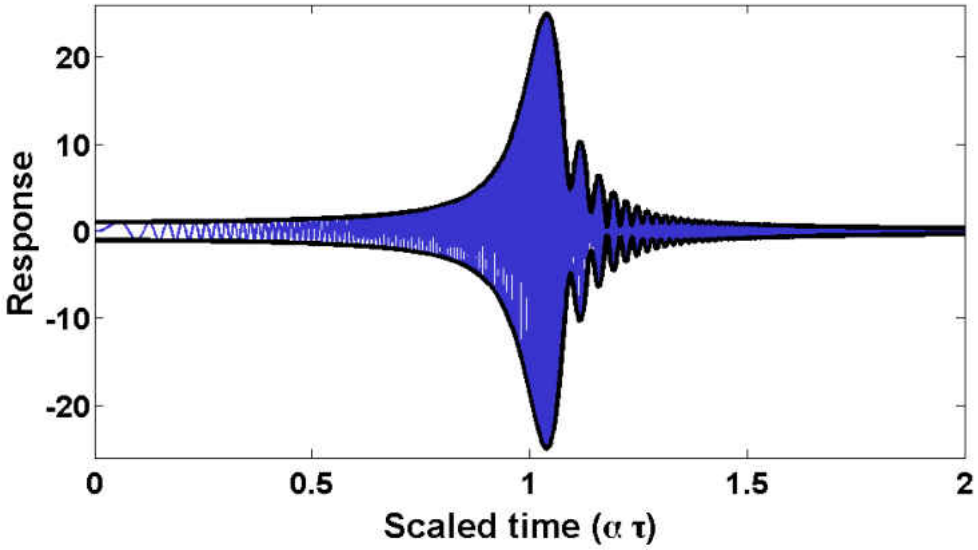

(a) *Response magnitude.*

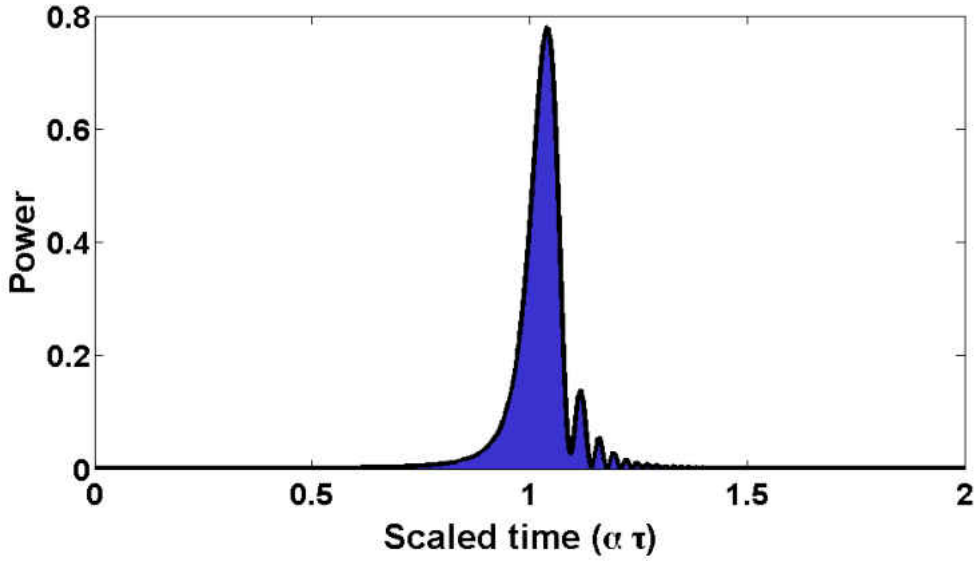

(b) *Power output.*

Figure 3.2: *Response and power output of a system subjected to frequency sweep excitations, for sweep rate* $\alpha = 10^{-3}$*, modal damping ratio* $\zeta = 0.1\%$*, and electromechanical coupling coefficient* $k^2 = 5.0\%$*.*

Alternatively, Equation (3.35) can be rewritten as

$$\{z'\} + [C]\{z\} = \{f\}, \tag{3.37}$$

where

$$[C] = [A]^{-1}[B], \tag{3.38}$$

and it can be easily verified that

$$[A]^{-1}\{f\} = \{f\}. \tag{3.39}$$

Using the method of integrating factors, a solution for this system can then be found:

$$\{z(\tau)\} = e^{-[C]\tau}\{z(0)\} + e^{-[C]\tau}\int_0^\tau e^{[C]\tau}\{f\}d\tau. \tag{3.40}$$

Here $e^{[C]\tau}$ is the matrix exponential, and a solution for the integral is still required. As can be verified by differentiation, this integral comes to

$$\int_0^\tau e^{[C]\tau}\{f\}d\tau = \mathrm{Im}\left\{\sqrt{\frac{-\pi}{2i\alpha}}e^{\frac{i}{2\alpha}\left(2\alpha\phi-\alpha_0^2+2i\alpha_0[C]+[C]^2\right)}\right. \tag{3.41}$$

$$\left.\cdot\left[\mathrm{erf}\left(\frac{[C]+i\alpha_0}{\sqrt{-2i\alpha}}\right)-\mathrm{erf}\left(\frac{i\alpha\tau+[C]+i\alpha_0}{\sqrt{-2i\alpha}}\right)\right]\right\}\begin{Bmatrix}1\\0\\0\end{Bmatrix}. \tag{3.42}$$

Complications arise when taking the error function of the matrix $[C]$, however. To see a possible reason for this difficulty, consider the definition of the error function:

$$\text{erf}(x) = \frac{2}{\sqrt{\pi}} \int_0^x e^{-t^2} dt. \tag{3.43}$$

The argument of the error function is thus the upper limit of an integral, and it is unclear how to proceed when the upper limit of an integral is a matrix. One possibility is to diagonalize the matrix,

$$[C] = [V][D][V]^{-1} \tag{3.44}$$

and then calculate the error function as

$$\text{erf}([C]) = [V]\text{erf}([D])[V]^{-1}. \tag{3.45}$$

CHAPTER 4
RESULTS

This chapter begins by examining steady-state energy harvesting near the open- and short-circuit conditions, as is required for effective implementation of resonance frequency detuning. The results of this work are then verified through a simple experiment, with theory and experiment in excellent agreement. Preceding to study energy harvesting behavior in a system with frequency sweep excitations, the next section develops a metric for using the harvested energy as a proxy for real-time knowledge of the blade vibration characteristics. Finally, as the frequency sweep rate does not appear in conventional energy harvesting research, the role of this parameter is studied in detail.

4.1 Harvesting at the Margins

Of interest here is developing an understanding of energy harvesting far from conventional harvesting conditions – that is far from resonance and near the open- and short-circuit conditions required for effective resonance frequency detuning. Considering Figures 4.1 and 4.2, it is readily seen that appreciable energy is a harvested over a small region of the R-Ω plane, as is well established in the field of piezoelectric-based energy harvesting. Cross sectional slices of Figure 4.2 are given in Figures 4.3 and 4.4. This result, it would seem, is rather discouraging for an application where we

seek to operate far from this subspace of efficient harvesting conditions. Note that, as Renno et al. discovered, the peak power output splits to a bimodal distribution as the damping ratio drops below the bifurcation damping ratio [29]. This result will be particularly useful as the problem is recast in terms of the effective structural stiffness derived in section 3.2.2.

This research effort is particularly interested in understanding how shifts in the effective stiffness near the open- and short-circuit conditions affect the power output. This relationship is expressed analytically in Equation (3.32) and plotted in Figure 4.5. Note the distinct change in the topology of the solution when the problem is recast in terms of the effective stiffness: there is now a significant region where appreciable energy is harvested. Indeed, a small shift in the effective stiffness near the open- and short-circuit conditions has a dramatic impact on the power output of the system. This is an excellent result for resonance frequency detuning, as it indicates that it will be possible to operate very near the ideal conditions of open- and short-circuit, while still harvesting adequate energy to trigger the change in stiffness states. While this result would very likely not be anticipated by even the most experienced energy harvesting researchers – who would tend to expect something of a bell curve – it is maybe not so surprising. To see why, consider Figure 2.4. Near the open- and short-circuit conditions, a shift of several orders of magnitude in the shunt resistance has a negligible on the effective stiffness, yet one would expect there to be an appreciable change in the power output of the system; thus, one can change the shunt resistance substantially to improve the power output while essentially maintaining the open-circuit and short-circuit stiffness states.

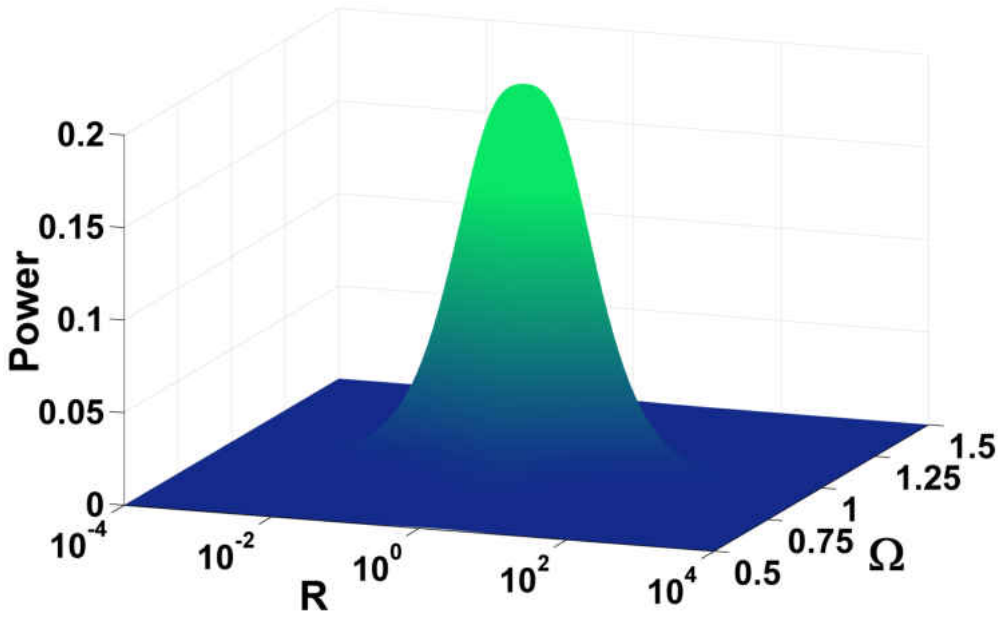

Figure 4.1: *Power output as a function of resistive load and frequency for* $\zeta = 1.5\%$ *and* $k^2 = 5\%$.

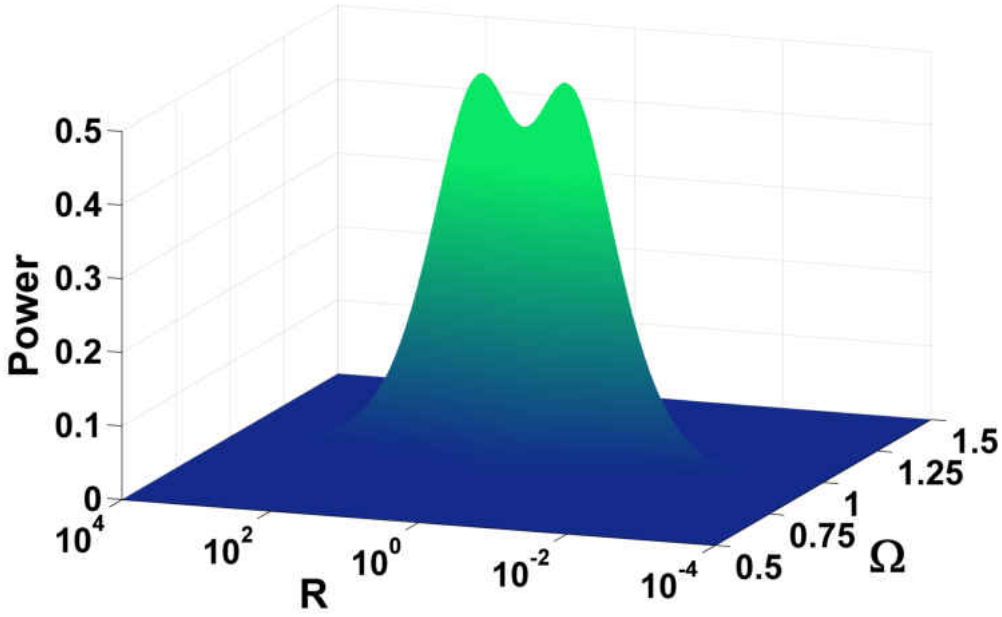

Figure 4.2: *Power output as a function of resistive load and frequency for* $\zeta = 0.6\%$ *and* $k^2 = 5\%$.

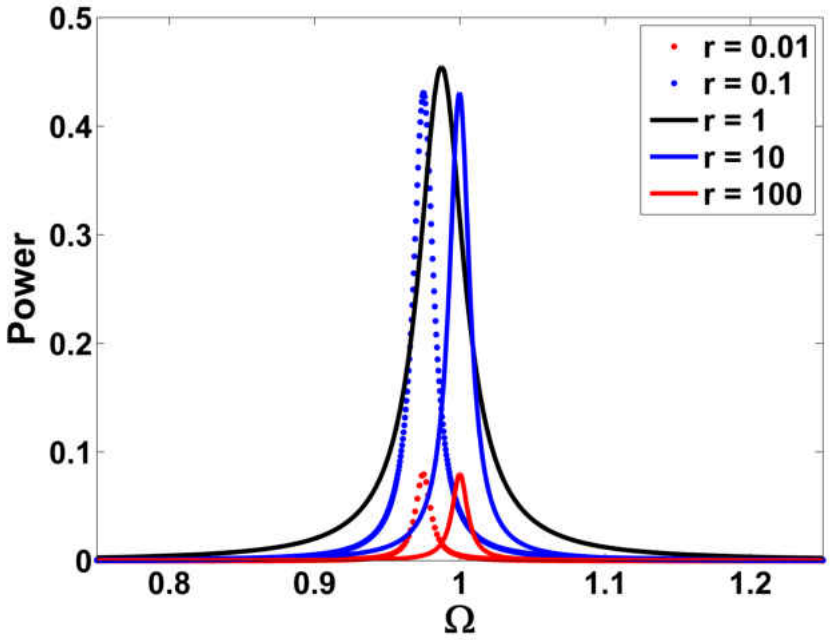

Figure 4.3: *Power output as a function of excitation frequency normalized by optimal power output, with* $\zeta = 0.6\%$ *and* $k^2 = 5\%$.

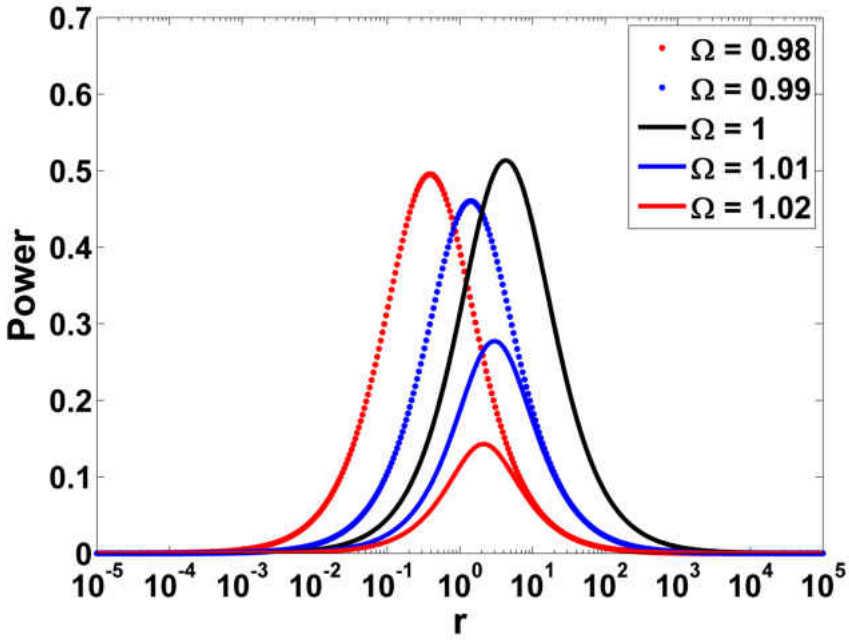

Figure 4.4: *Power output as a function of resistive load normalized by optimal power output, with* $\zeta = 0.6\%$ *and* $k^2 = 5\%$.

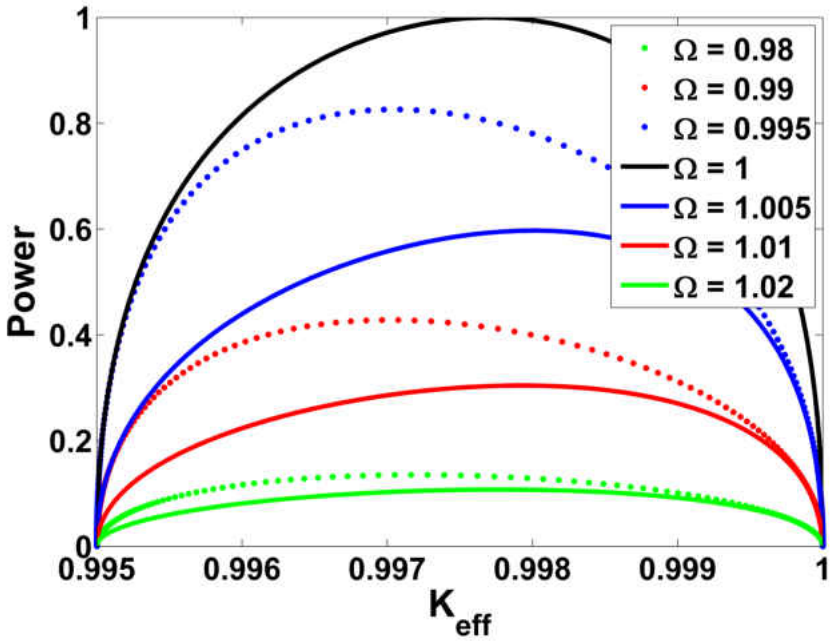

Figure 4.5: *Power vs. effective stiffness for several driving frequencies, normalized by the optimal power output, with* $\zeta = 0.6\%$ *and* $k^2 = 5\%$.

4.1.1 Ultra Low Damping

In light of the previous discussion on monolithic blade construction, the case of ultra low damping is of particular interest here. Figures 4.6 and 4.7 shows the power output for a (relatively) high damping ratio and for a very low damping ratio (though certainly within the region of observed values for a typical blade). We see that the power output is significantly increased in the low damping case. More importantly, the peak power output has bifurcated, with the two peaks moving near the margins – that is at high and low stiffness states, corresponding to approximately open- and

short-circuit. As a result, the sensitivity of the power output to stiffness changes near the margins is enhanced in the low damping case, behavior that can be taken advantage of in this application.

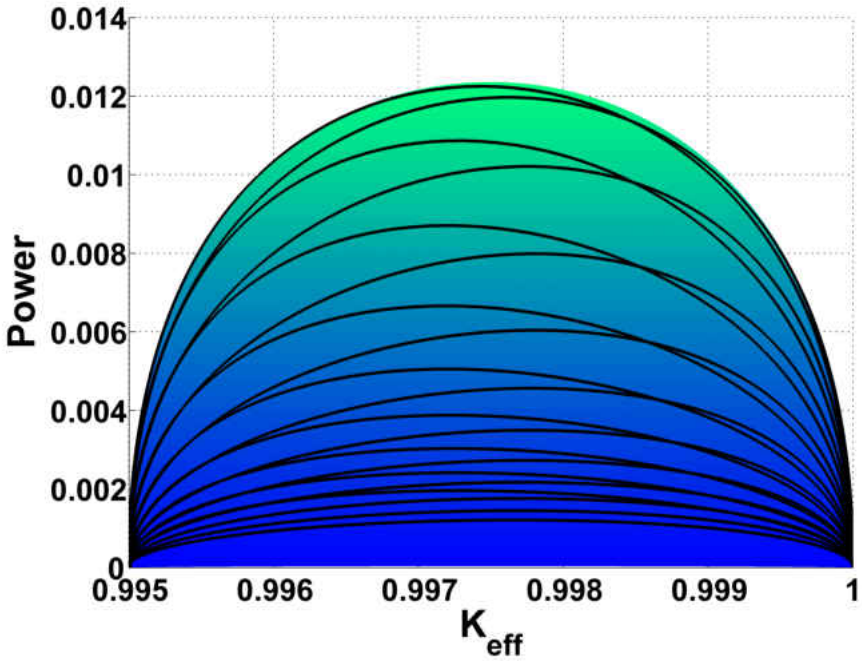

Figure 4.6: *Power output as a function of effective stiffness, for* $\Omega \in [0.5 : 1.5]$ *and* $k^2 = 5\%$. *(Relatively) high damping case,* $\zeta = 6\%$. *Note the difference in the scale on the vertical axis.*

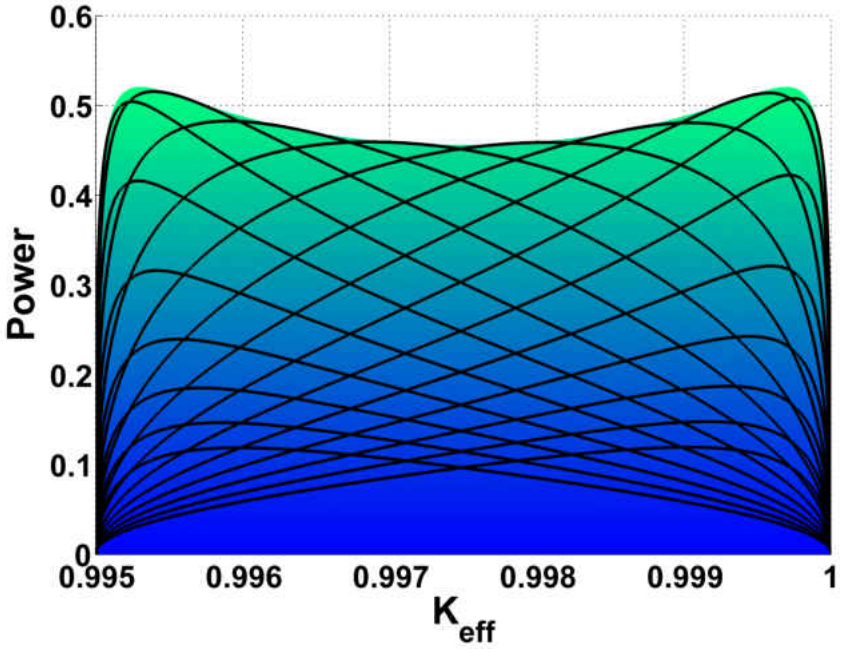

Figure 4.7: *Power output as a function of effective stiffness, for* $\Omega \in [0.5 : 1.5]$ *and* $k^2 = 5\%$*. Ultra low damping case,* $\zeta = 0.06\%$*. Note the difference in the scale on the vertical axis.*

4.1.2 Experimental Validation

Though the focus of this work was theoretical, a brief experiment was performed to validate the results of the model in this steady-state analysis.

4.1.2.1 Experimental Setup

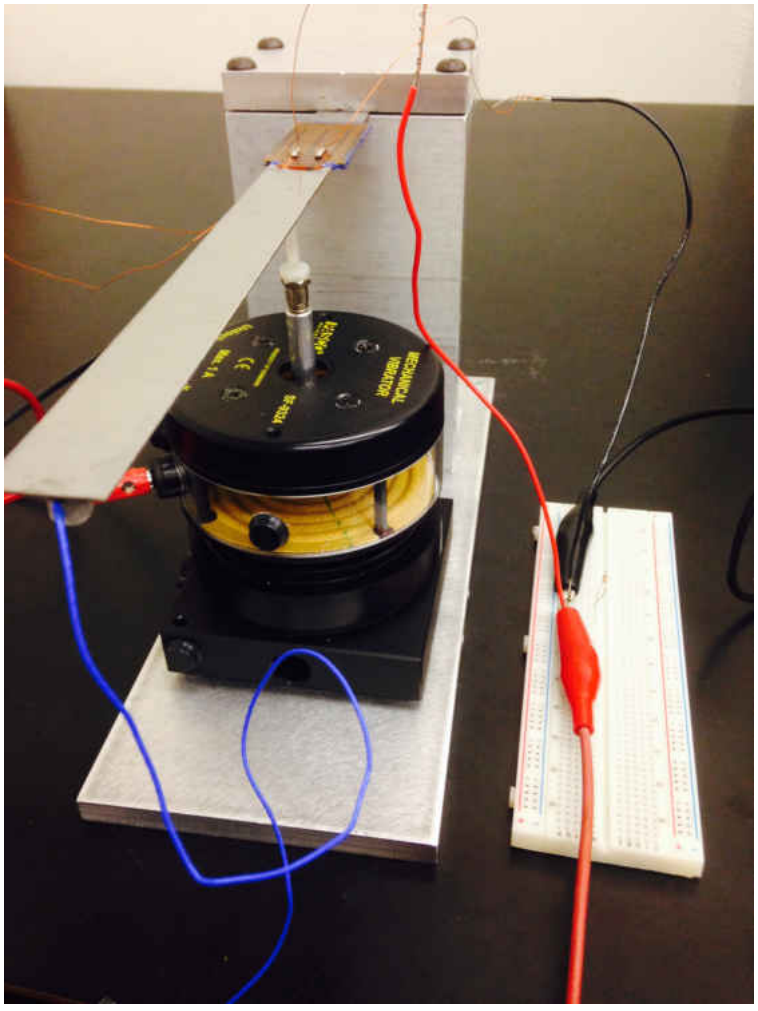

Figure 4.8: *Experimental setup.*

The experimental setup used to confirm the experimental results of the previous sections consisted of a steel cantilever beam mounted to a rigid base structure. A pair of Midé qp10n piezoelectric actuators were bonded near the base of the beam in a bimorph configuration and connected in parallel to a resistive shunt attached to a breadboard. Each Midé piezoelectric element has a nominal capacitance of $C_o = 55$ nF. The experimental setup can be seen in Figure 4.8. For data acquisition, MATLAB's Data Acquisition Toolbox was used in conjunction with an NI-9234 DAQ device. The acceleration of the beam was measured by an accelerometer attached at the tip, and the NI DAQ device recorded the voltage across the piezoelectric element as well as the voltage associated with the excitation.

Before conducting any experimental investigation, it was necessary to determine the coupling coefficients k^2, the damping ratios ζ, and the open-circuit natural frequencies f_n of the first several modes. To this end, the structure was excited at the base via an impact hammer, and a simple circle fit along with the half-power bandwidth method sufficed to determine the damping ratios, the natural frequencies at both open- and short-circuit, and thus the coupling coefficients (recall the definition of the coupling coefficient given by Equation (2.6)). The results are displayed in Table 4.1.

4.1.2.2 Experimental Results

Table 4.1: *Modal Parameters*

$f_{n,\text{oc}}$ [Hz]	ζ_n	k^2
12.8	0.8%	2.5%
68.06	0.6%	0.5%
192.09	0.2%	0.1%
398.3	0.9%	0.7%

Seeking to validate the analytical results of Equation (3.19) (as seen in Figure 4.4), the structure was excited at the resonance frequency of the second vibration mode, $f_{2,\text{oc}} = 80$ Hz. These excitations were generated by a shaker attached near the base of the beam (see Figure 4.8), and the second mode was chosen because the relatively primitive shaker used was observed to produce the cleanest signal near this frequency. The power dissipated across the shunt was calculated as the square of the voltage measured across the resistor divided by the shunt resistance. By varying the shunt resistance over a number of values between open- and short-circuit, the experimental dependence of the power on shunt resistance was determined. Displayed in Figure 4.9, the theory and experimental results are seen to agree quite well. For lack of a better method, the effective beam stiffness was then calculated from the experimental values of k^2, R, and Ω via the theoretical definition in Equation (3.28), in an effort to validate the results of Figure 4.5. The results are displayed in Figure 4.10, and, again, close agreement between theory and experiment is observed. This is particularly true near the open- and short-circuit conditions – the "margins," precisely the conditions which are of prime interest in this research.

This discussion would be incomplete without mentioning potential sources of error in this experiment, of which there are several. One such source is the precision of the instruments used for measurement – for example the DAQ device, the accelerometer, the interfacing between the DAQ device and MATLAB. Another source of error comes from environmental factors – vibrations in the building (particularly when not on the ground floor, as was the case in this experiment), temperature fluctuations, someone bumping the table containing the experimental setup. Yet another source of error arises from the fact that the theoretical model is derived from the assumption of base excitations, which were not possible to reproduce in practice due to the limited equipment that was available at the time – with a full scale shaker issue can be alleviated in the future. Finally, one expects that there should be a more convincing method to determine the effective stiffness experimentally, rather than relying on the theoretical result. It is no wonder that Figure 4.10 shows close agreement between theory and experiment, as it is simply a reparameterization of the results in Figure 4.9. One possibility would be to statically load the beam and record the tip deflection for many shunt resistances, as the deflection should be proportional to the effective beam stiffness. To accurately achieve this, however, it is important to have a structure with high coupling, as the shift in stiffness between open-circuit and short-circuit needs to be of sufficient magnitude that the variation in beam deflection is appreciable.

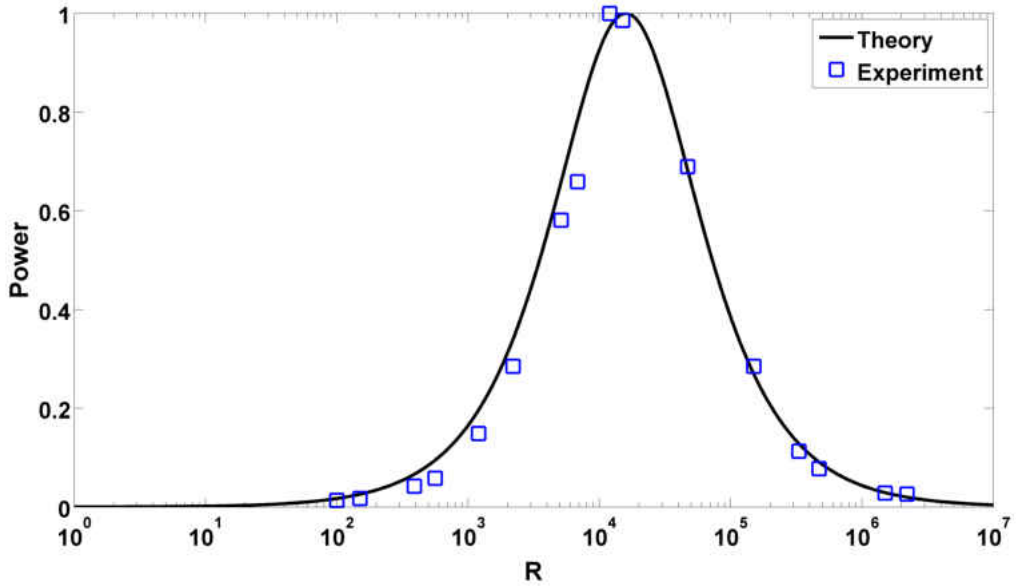

Figure 4.9: *Comparison of analytical results with experiment for the dependence of power output on shunt resistance, for* $k^2 = 0.5\%$, $\zeta = 0.6\%$, *and* $\Omega = 1$.

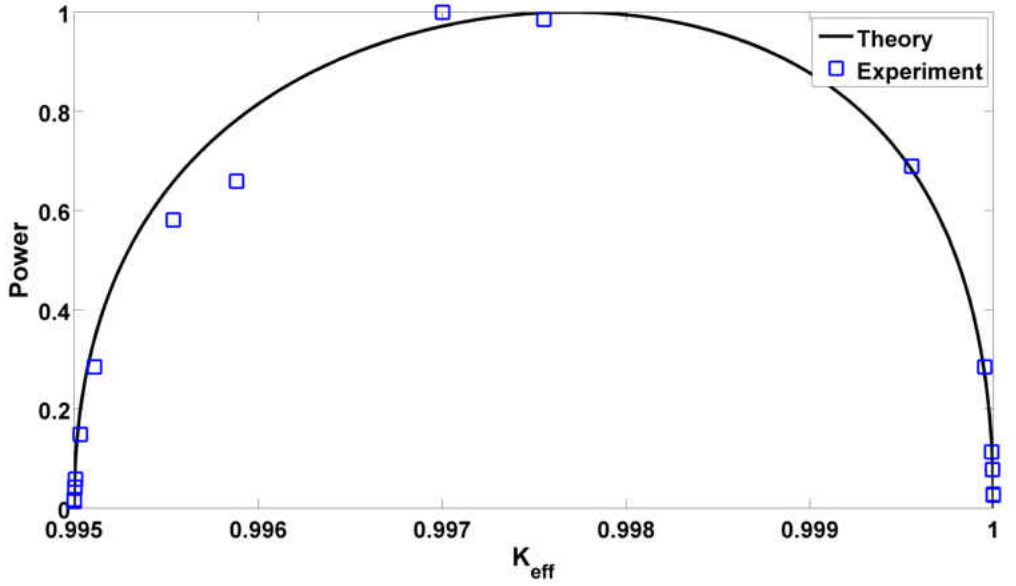

Figure 4.10: *Comparison of analytical results with experiment for the dependence of power output on effective stiffness, for* $k^2 = 0.\%5$, $\zeta = 0.6\%$, *and* $\Omega = 1$.

4.2 Harvesting as a Proxy for Vibration Characteristics

A practical implementation of resonance frequency detuning in the turbomachinery environment will allow for minimal on-blade sensing and processing, and a quantity readily measured on-blade that can serve as a proxy for real-time knowledge of the local vibration characteristics is sought. One such quantity that immediately presents itself is the harvested energy, which, by the nature of the electromechanical coupling exhibited by piezoelectric materials, must be closely correlated with the vibration history. It is already necessary to store the energy as it is being harvested, and it may be that some threshold harvested energy can serve as a trigger for the optimal switch in the control law inherent to resonance frequency detuning. This section seeks to minimize the response of the system in terms of the harvested energy at the time of the switch, developing a metric for using the harvested energy to optimally trigger the change in stiffness states with little signal processing or additional hardware needed. Here the optimal switch is defined as that which minimizes the peak response of the system, though there are several other possible definitions of optimality – for example minimizing the total area under the response curve or maximizing the speed at which the oscillations in the response envelope decrease below some threshold value.

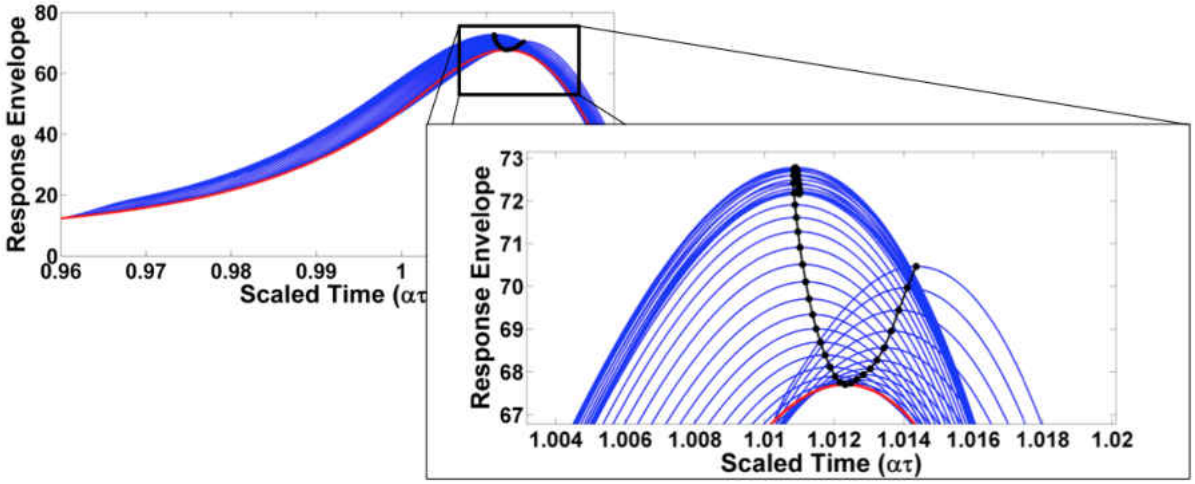

Figure 4.11: *Response envelopes for a many switching times. The optimal (minimized) response is given in red, as well as the peak response corresponding to each switch time, for* $\alpha = 10^{-4}$, $k^2 = 1.0\%$, $\zeta = 0.5\%$, $r_{oc,sc} = 10^{\pm 3}$.

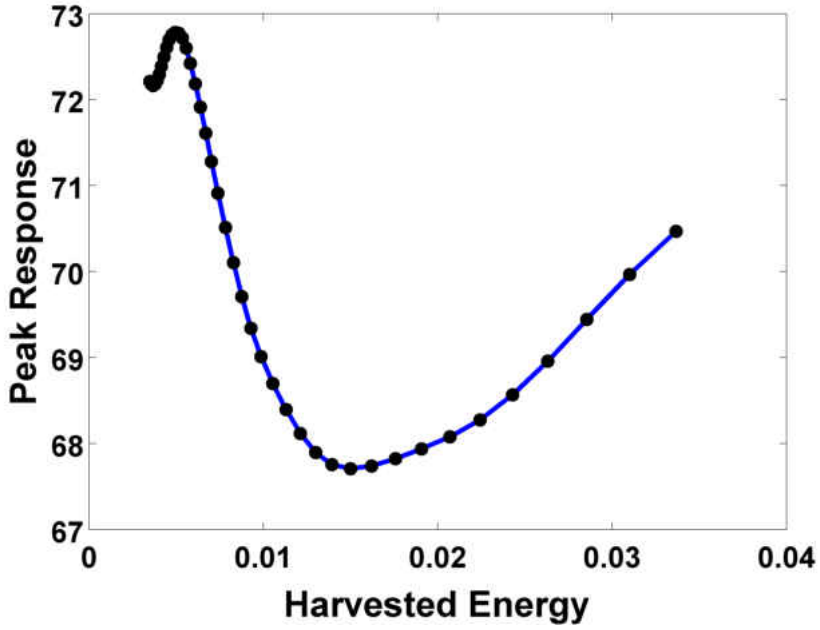

Figure 4.12: *Peak response vs. energy harvested at the time of the switch, for* $\alpha = 10^{-4}$, $k^2 = 1.0\%$, $\zeta = 0.5\%$, $r_{oc,sc} = 10^{\pm 3}$.

In developing a proxy relationship between the harvested energy and mechanical response of the blade, the system was first simulated for a number of different switch times, saving the energy harvested at the time of the switch for each case. The response curves for each switch trigger are shown in Figure 4.11, where black dots indicate the peak response of each case and the optimal curve (minimal response) is in red. Each peak response is then plotted in terms of the energy harvested at the switching time, as in Figure 4.12, essentially reparametrizing the problem in terms of the harvested energy rather than the switch time. Figure 4.12 shows a clear minimum in the response for a nondimensional energy of about 0.015, establishing that the harvested energy can indeed be used to indicate the switch time which minimizes the peak response of the system. This optimal switching energy is expected to depend on the key parameters of the system, namely the coupling coefficient, the modal damping ratio, the sweep rate, and the open- and short-circuit shunt resistances. Recall that true open- and short circuit conditions allow for no energy harvesting, and when refered to in this context open-circuit and short-circuit refer to shunts which approximate these conditions through very high and very low resistances, respectively. To clarify the notation used in this section, $r_{\text{oc,sc}} = 10^{\pm N}$ refers to an open-circuit resistance of $r_{\text{oc}} = 10^{N}$ and a short-circuit resistance of $r_{\text{sc}} = 10^{-N}$.

Having established that the harvested energy does indeed seem to be a potential metric for the optimal switch in resonance frequency detuning, the simulation was repeated for six sets of open- and short-circuit shunt resistances ranging between $r_{\text{oc,sc}} = 10^{\pm 4}$ in an effort to understand how this optimal switching energy depends on the shunt resistances. Proceeding in the same manner as before, the peak response for each switch trigger is plotted against the harvested energy at the

time of the switch in Figure 4.13; in each case it is clear that the response in minimzed at some optimal switching energy. Seeking to remove the dependence on shunt resistance, both the vertical and horizontal axes were then normalized. The peak response of each switch time was normalized by the peak response of the unswitched system – that is, the system with no detuning applied, while the harvested energy is normalized by a characteristic energy at the switching time. This quantity is constructed as the product of the switching time and the instantaneous power at the switching time, while this power is calculated as the square of the piezoelectric voltage at the switch divided by the resistance immediatetly before the switch – that is, the open-circuit resistance. However, the same switching times were used in the simulations for each set of open- and short-circuit resistances, and the voltage is known at the time of the switch, therefore this charactersitic energy can simply be written as a constant over the open-circuit resistance:

$$E^* = \frac{V_{\text{switch}}^2}{r_{\text{oc}}} \tau_{\text{switch}} \sim \frac{C}{r_{\text{oc}}} \tag{4.1}$$

Figure 4.14 shows the results of this normalization; observe that the six peak repsonse curves have collapsed to a single curve, indicating that this normalized switching energy is independent of the shunt resistance used. Note how, if the switch is applied too early, the peak response of the detuned system can exceed that of the system with no switch; a proper selection of the swich time is indeed very important.

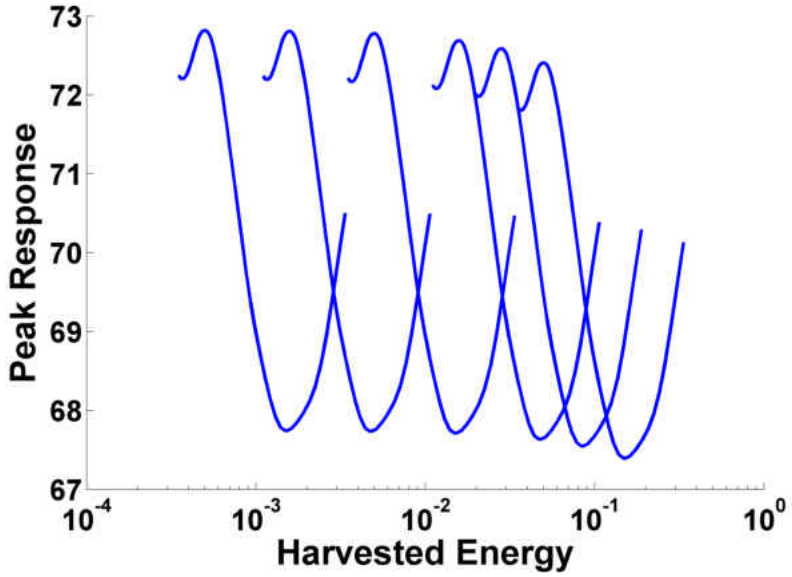

Figure 4.13: *Peak response as a function of harvested energy at the time of the switch, for sweep rate* $\alpha = 10^{-4}$*, modal damping ratio* $\zeta = 0.1\%$*, electromechanical coupling coefficient* $k^2 = 5.0\%$*, and 6 different sets of shunt resistances ranging between* $r_{oc,sc} = 10^{\pm 4}$ *and* $r_{oc,sc} = 10^{\pm 2}$.

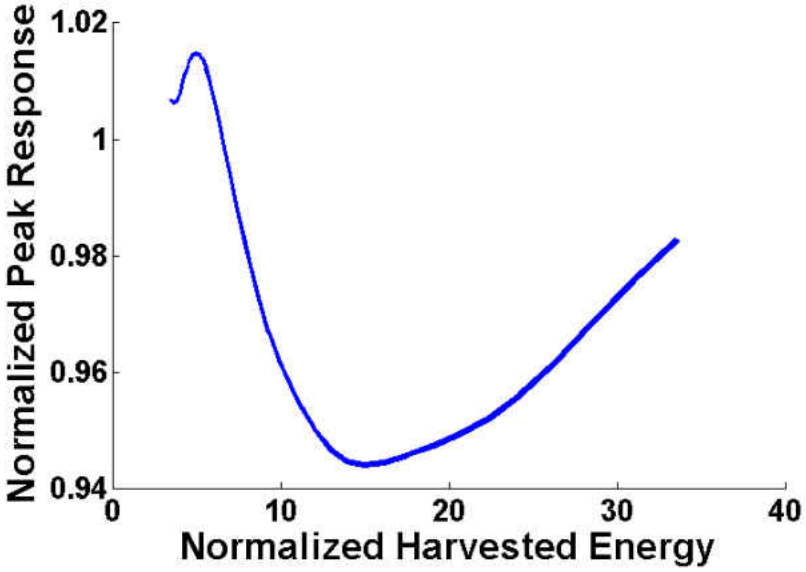

Figure 4.14: *Normalized peak response as a function of normalized harvested energy at the time of the switch, for sweep rate* $\alpha = 10^{-4}$*, modal damping ratio* $\zeta = 0.1\%$*, electromechanical coupling coefficient* $k^2 = 5.0\%$*, and 6 different sets of shunt resistances ranging between* $r_{oc,sc} = 10^{\pm 4}$ *and* $r_{oc,sc} = 10^{\pm 2}$.

Having eliminated the optimal switching energy's dependence on the shunt resistances, the effects of changing the other key parameters – the coupling coefficient, sweep rate, and damping ratio – are now investigated by repeating the process described above for a range of values of each parameter: $\alpha \in \left[10^{-5}, 10^{-3}\right]$, $\zeta \in [0.05\%, 1\%]$, and $k^2 \in [1\%, 10\%]$. By varying each parameter independently while holding the other parameters constant at the nominal values of $\alpha = 10^{-4}$, $\zeta = 0.1\%$, and $k^2 = 1.0\%$, the effect each parameter has on the optimal switch energy was clearly observed, as can be seen in Figures 4.15 to 4.17. For each of these cases the simulation was repeated for the open- and short-circuit resistances $r_{\text{oc,sc}} = 10^{\pm 2}$ and $r_{\text{oc,sc}} = 10^{\pm 3}$ to confirm the above result that the same optimal normalized switching energy is found for different choices of the shunt circuit resistances.

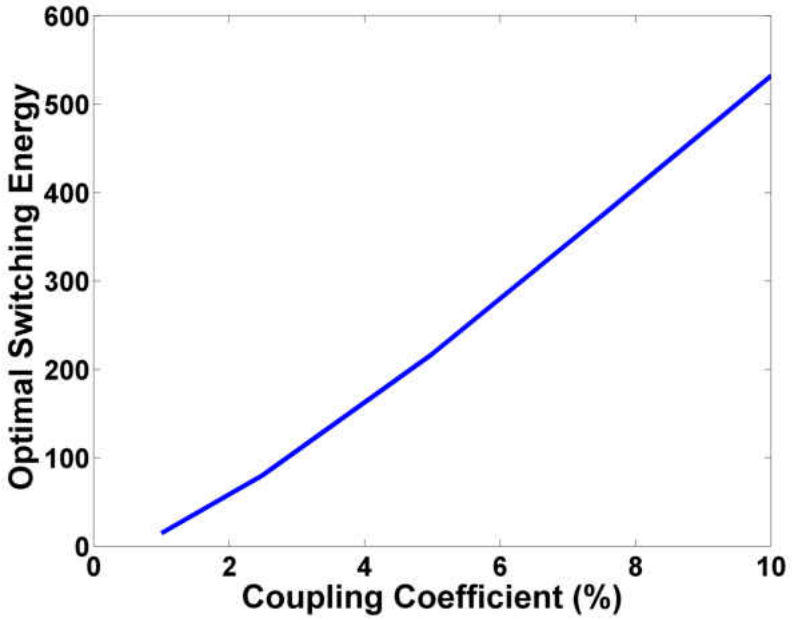

Figure 4.15: *Optimal switching energy vs. coupling coefficient, for* $\alpha = 10^{-4}$, $\zeta = 0.5\%$.

The effect of varying each of these parameters is now considered in turn. It is readily seen in Figure 4.15 that increasing the coupling coefficient leads to an increased optimal switching energy, behavior that can be understood intuitvely by considering that increased coupling means the structure is able to convert more strain energy to electrical energy. As a result, more energy will be harvested for a given switching time as the coupling coefficient increases. Figure 4.16 shows that increasing the sweep rate causes the optimal switching energy to quickly decrease, again, behavior that makes sense. Increasing the sweep rate means that resonance is reached more rapidly, thus less time is spent harvesting before the switch and the optimal switching energy accordingly decreases. More precisely, one would expect the switch to occur at approximaetely the same frequency (equivalently, the scaled time $\alpha\tau$) regardless of the sweep rate, thus the time the switch occurs scales with α^{-1}. Finally, Figure 4.17 shows that decreasing the modal damping ratio causes the optimal switching energy to increase. Once again, this is logical bahavior. It is commonly known that the mechanical response of a system increases for a decreasing damping ratio, therefore more strain energy is present for the energy harvesting system to convert to electrical energy. As a result, even if the switch time were independent of the damping ratio – which it is not – the energy harvested at the time of the switch would increase for a decreased damping ratio [38].

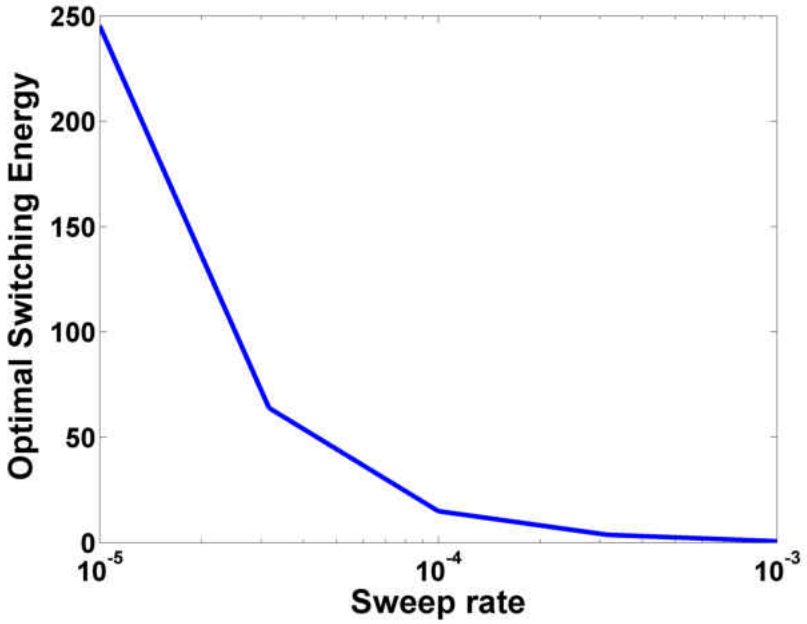

Figure 4.16: *Optimal switching energy vs. sweep rate.* $k^2 = 1.0\%$, $\zeta = 0.5\%$.

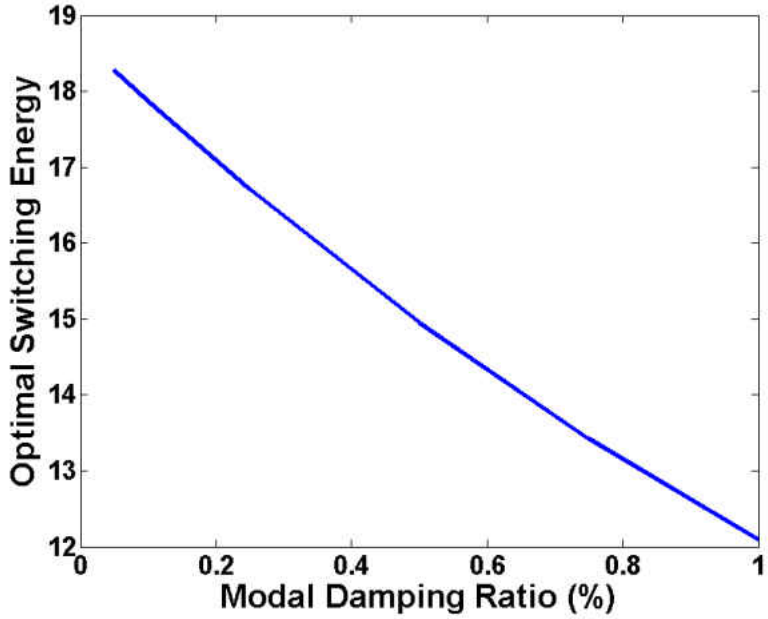

Figure 4.17: *Optimal switching energy vs. modal damping ratio, for* $\alpha = 10^{-4}$, $k^2 = 1.0\%$.

4.3 The Role of Sweep Rate

The frequency sweep rate, α, has been seen to have an impact on transient energy harvesting behavior in the previous section, and its role is investigated in more detail here. As resonance frequency detuning is formulated for systems with a changing excitation frequency, it is important to understand the role of the sweep rate, the parameter that describes the rate at which the excitation frequency changes. Considered here are only linear frequency sweeps, though higher order sweeps could be handled analogously.

The nondimensional sweep rate used in this work, α, can be expressed for each vibration mode in terms of the dimensional sweep rate and the resonance frequency of the mode of interest: [8]

$$\alpha = \frac{f_{\text{rate}}}{2\pi f_n^2} \tag{4.2}$$

This expression allows us to establish a typical range of sweep rates in turbomachinery applications. Consider a machine with a rotation sweep rate of 3000 RPMs, corresponding to approximately 50 Hz/s. In exciting a resonance at 100 Hz, the sweep rate is $\alpha \approx 10^{-3}$; in exciting a resonance at 1000 Hz, the sweep rate is $\alpha \approx 10^{-5}$. Higher sweep rates can be generated through higher engine order excitations (denoted by N in Figure 1.3), but this exercise establishes a baseline range to investigate.

To understand the role of the frequency sweep rate in transient energy harvesting systems, first consider Figure 4.18, where the power output is plotted as a function of the resistive load and the instantaneous excitation frequency. Several important observations can be made. The figure shows

that as the sweep rate decreases the peak power output of the system increases and the peak becomes much sharper. This behavior is reminiscent of the role the modal damping ratio plays in mechanical systems, as a decreasing damping ratio leads to increased peak response as well as a sharper, more narrow, peak. Drawing further analogy with the damping ratio, recall that Renno et al. found that the optimal power output bifurcates as the damping ratio drops below a particular value, called the bifurcation damping ratio [29]. Again, we see very similar behavior here. When the sweep rate drops below $\alpha = 10^{-3}$, we begin to see two distinct maxima in the power output, corresponding to the resonance and anti-resonance. We can then say there is a 'bifurcation sweep rate,' which depends on the other key parameters of the system – the damping ratio and the coupling coefficient.

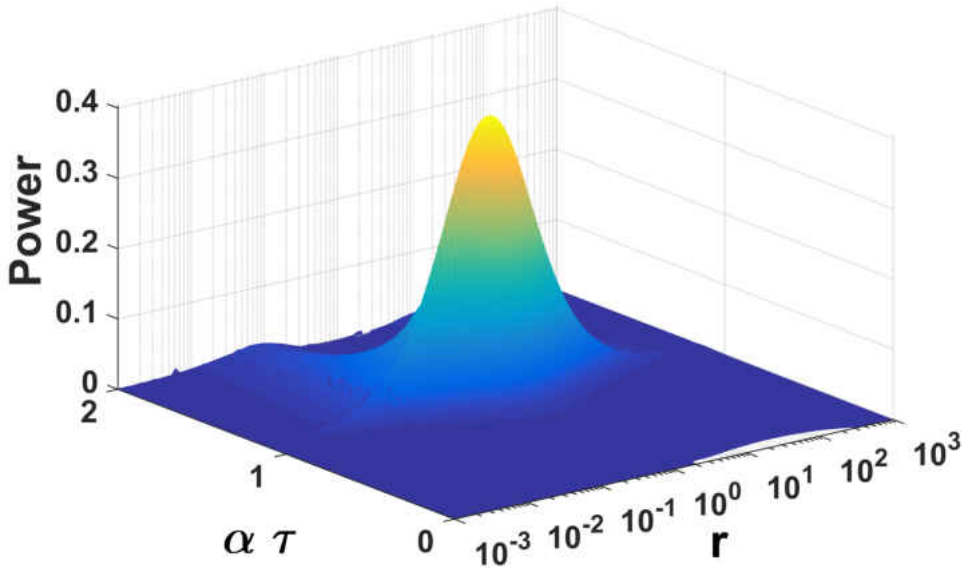

(a) $\alpha = 10^{-2.5}$

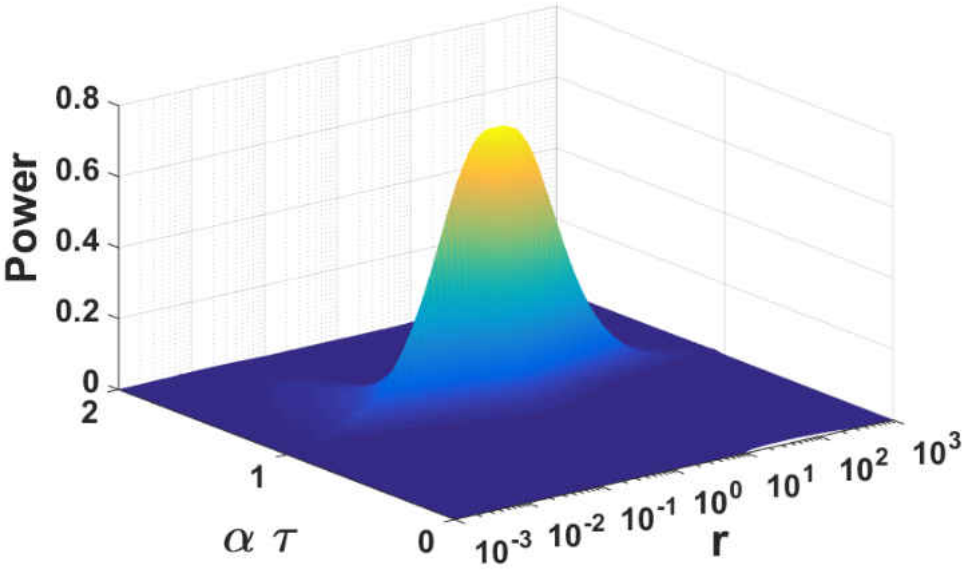

(b) $\alpha = 10^{-3}$

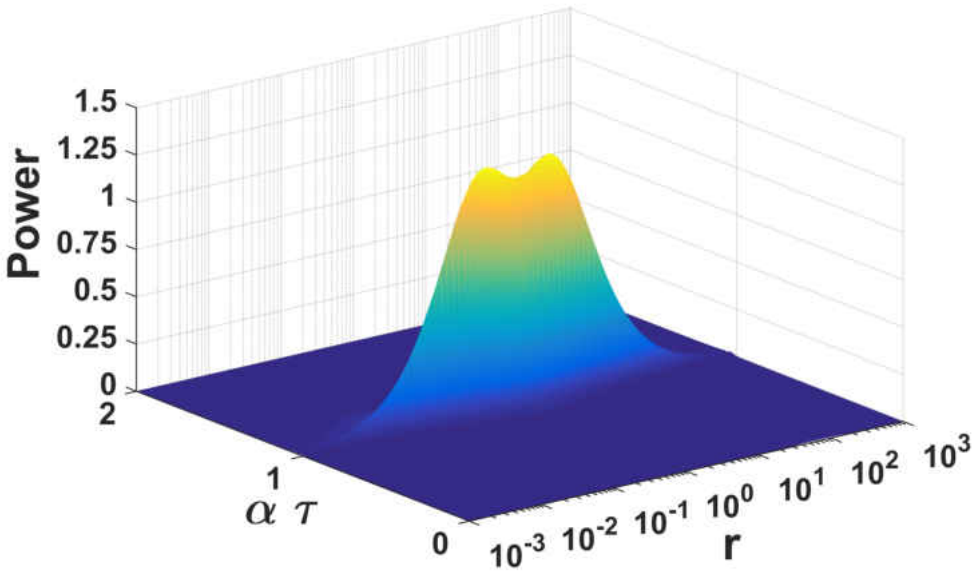

(c) $\alpha = 10^{-3.5}$

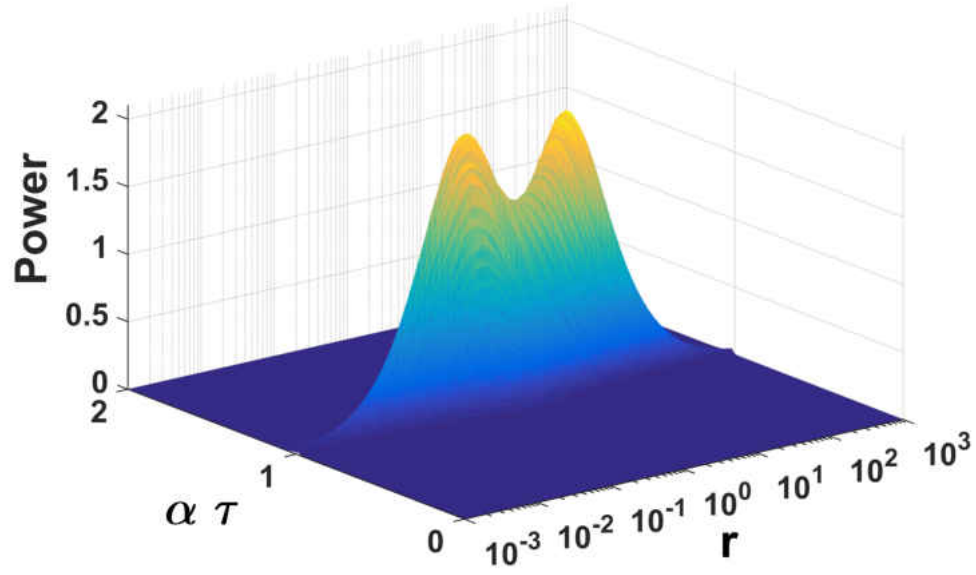

(d) $\alpha = 10^{-4}$

Figure 4.18: *Power output vs. shunt resistance and instantaneous frequency (scaled time), for* $\zeta = 0.1\%$ *and* $k^2 = 5\%$*. Note the different scales on the vertical axes.*

To further develop an understanding of the effect of the sweep rate, now consider Figure 4.19. Figure 4.19a is a bifurcation diagram showing how the optimal shunt resistance depends on the sweep rate. For high sweep rates, there is a single optimal value of the resistance, corresponding of course to the peak power output. As the sweep rate decreases, however, three distinct extrema arise: two local maxima and a minimum. Refer to Figure 4.18d for a clear depiction of this behavior for a particular value of the sweep rate ($\alpha = 10^{-4}$). Figures 4.19b and 4.19c show how the extremal values of the power output and mechanical response vary with the sweep rate. The resonance and anti-resonance show very similar behavior, with the resonance having a slightly larger value for each the power output and mechanical response. The local minimum, however, seems to plateau to a constant value as the sweep rate approaches zero. This observation may be justified by considering that as the sweep rate approaches zero we expect to recover steady state behavior, and it seems that the minimum is indeed converging toward some value as the sweep rate approaches zero.

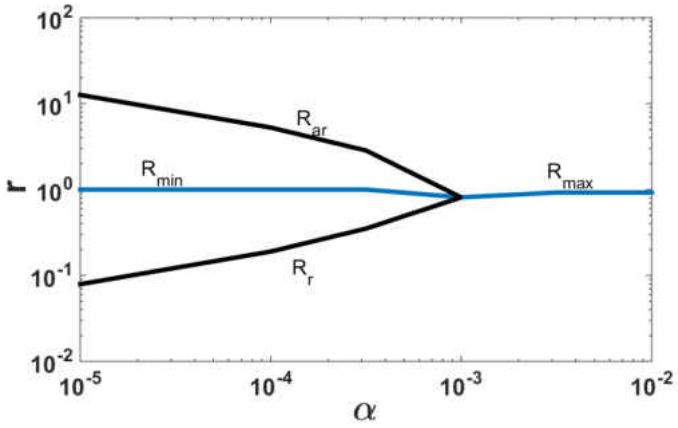

(a)

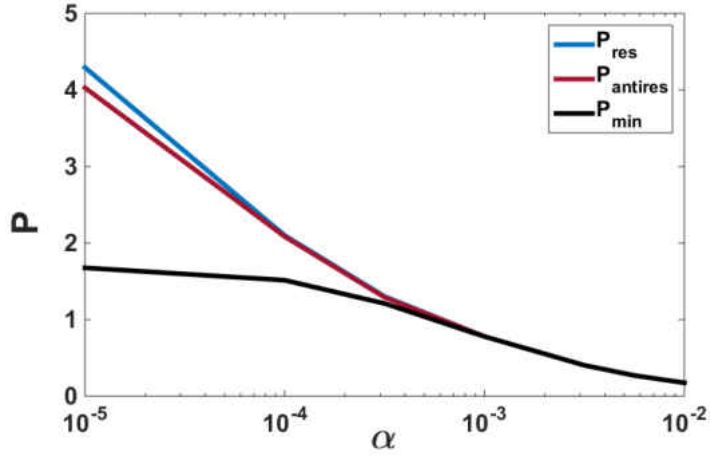

(b)

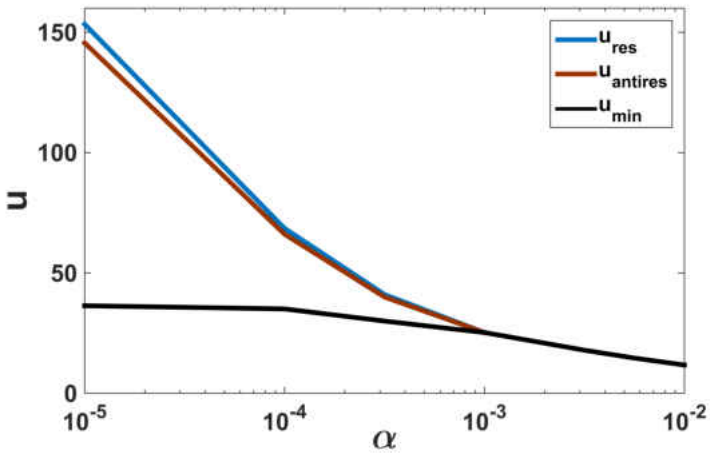

(c)

Figure 4.19: *Depiction of local extrema for shunt resistance, power output, and mechanical response as a function of the sweep rate, for* $\zeta = 0.1\%$ *and* $k^2 = 5\%$.

CHAPTER 5
CONCLUSIONS

The purpose of this work was to improve the understanding of energy harvesting behavior in the context of a vibration reduction method for turbomachinery bladed disks, namely resonance frequency detuning. This method only requires a small amount of power to alter the boundary conditions of the piezoelectric material, and thus this work differs from much energy harvesting research in that it is not concerned with maximizing the power output of the system.

Resonance frequency detuning is most effective when the stiffness states are well separated, a condition that is met when the open- and short-circuit boundary conditions are used. These states correspond to zero charge displacement and zero voltage, however, and therefore no energy flow. The first step was thus to examine energy harvesting behavior far from optimal harvesting conditions – near open- and short-circuit. An expression relating the electrical impedance in the harvesting circuit to the effective structural stiffness was developed, showing that a continuous distribution of stiffness states is available by varying the impedance. The power output of the system was then studied in terms of this effective structural stiffness, finding that a small shift in stiffness near the open- and short-circuit conditions leads to a significant increase in power output. Encouragingly, this effect is amplified in the case of ultra low damping, one of the precise conditions that necessitates this vibration reduction technique.

In considering practical on-blade implementation of resonance frequency detuning, size becomes an important factor. With this limitation in mind, it is desirable to minimize the need for sensors and on-blade signal processing, and, as the energy is harvested from the local vibrations, it is clear that the harvested energy should be closely correlated with the vibration characteristics of the blade. One distinct possibility is therefore to use the energy harvested as a proxy for knowledge of the local vibration characteristics, a topic which was investigated in this work. Through time integration of the equations of motion, it was established that the optimal switch in the control law inherent to resonance frequency detuning could, at least in theory, be determined from the energy harvested. As a result it may be possible to use threshold stored energy to trigger the switch in stiffness states, eliminating the need for real-time knowledge of the mechanical behavior of the system as well as requiring minimal signal processing. It was found that the harvested energy corresponding to the optimal change in stiffness states is, after normalization, independent of the choice of open- and short-circuit resistances, effectively reducing the parameter space for further parametric studies of the relation between harvested energy and optimal switching for resonance frequency detuning.

5.1 Recommended Future Work

There are always opportunities to pursue further research, and this work would be incomplete without mentioning several possibilities. In continuing the study of energy harvesting "at the margins," a next step is to develop the circuitry needed to combine open- and short-circuit harvesting in a single system, allowing for control of the electrical boundary conditions and thus the stiffness states. It

has been shown that sufficient energy to change stiffness states is available under these non-optimal harvesting conditions; it now remains to accommodate both conditions in a unified approach. It would also be valuable to allow for other boundary conditions, as it may be found that it is necessary to alter the stiffness state slowly and continuously to avoid exciting higher modes – a sudden change in stiffness states may just as well push another vibration mode closer to resonance. Furthermore, as resonance frequency detuning is inherently an approach for control of transient vibrations, this analysis will need to extend to systems with a changing excitation frequency. It is anticipated that the sensitivity of power output near the open- and short-circuit conditions will remain a feature of systems with transient vibrations; however, this belief should be confirmed.

Several assumptions are made in this analysis for simplicity, providing several further topics for study as each of these assumptions are relaxed. It was idealized that the change in stiffness states occurs instantaneously, with the effect of continuous change in stiffness states over a finite time being neglected. It would be interesting to observe what effect such a switch has on the mechanical response of the system. In reducing the full blade dynamics model to the simplified equations of motion used throughout this work, a single-degree-of-freedom assumption was made, neglecting the effect state switching might have on exciting other vibration modes; in the future this analysis should extend to multi-degree-of-freedom systems.

An additional application of these results would be to detune a simple cantilever beam with base excitations as it passes through resonance, using the energy stored on a capacitor to trigger the switch as some threshold value is reached. This experiment would require developing the circuitry needed to process the harvested energy and trigger the change in boundary conditions in real time.

Given full knowledge of the system parameters, which is of course practical in the lab setting, the results of this work could be used to determine the optimal switching energy for a particular system. This approach is not realistic for actual implementation of resonance frequency detuning, however, particularly as many of the parameters are frequency dependent and thus constantly changing, and a deeper parametric study of the relationship between the harvested energy and the optimal switch is needed to develop a uniform metric for predicting the optimal switch trigger.

APPENDIX A
DERIVATION OF NONDIMENSIONAL EQUATIONS OF MOTION

The simplified equations of motion are derived from the full blade dynamics model:

$$\begin{bmatrix} M_m & 0 \\ 0 & 0 \end{bmatrix} \begin{Bmatrix} \ddot{w}_m \\ \ddot{w}_e \end{Bmatrix} + \begin{bmatrix} C_m & 0 \\ 0 & 0 \end{bmatrix} \begin{Bmatrix} \dot{w}_m \\ \dot{w}_e \end{Bmatrix} + \begin{bmatrix} K_m + \Omega^2 K_g & -K_c^t \\ -K_c & K_e^{-1} \end{bmatrix} \begin{Bmatrix} w_m \\ w_e \end{Bmatrix} = \begin{Bmatrix} F_m \\ F_e \end{Bmatrix}. \tag{A.1}$$

Several assumptions are then made: the modes are assumed to be well separated and thus the mechanical and electrical degrees of freedom can be considered as scalar quantities; the mechanical excitation is idealized as a swept sinusoidal force with constant amplitude; finally, the range of operating frequencies is restricted such that the geometric stiffening term is assumed to be constant in time. With these assumptions and some rearranging, we have,

$$\begin{aligned} M\ddot{x} + C\dot{x} + K_{\mathrm{oc}}x - K_{\mathrm{c}}Q &= f\sin(\omega t) \\ -K_{\mathrm{c}}x + \frac{1}{C_o}Q &= V \end{aligned} \tag{A.2}$$

Under short-circuit conditions (that is, $V = 0$), the second equation reduces to

$$Q = K_{\mathrm{c}}C_o x. \tag{A.3}$$

Upon substituting this expression in the first line of Equation (A.2), we have a form of the canonical second-order ordinary differential equation:

$$M\ddot{x} + C\dot{x} + (K_{\mathrm{oc}} - K_{\mathrm{c}}^2 C_o)x = f\sin(\omega t). \tag{A.4}$$

The short-circuit stiffness is therefore given by:

$$K_{\mathrm{sc}} = K_{oc} - K_{\mathrm{c}}^2 C_o. \tag{A.5}$$

Now, under short-circuit conditions (that is, $Q = 0$), Equation (A.2) becomes

$$\begin{aligned} M\ddot{x} + C\dot{x} + K_{\mathrm{oc}}x &= f\sin(\omega t) \\ -K_{\mathrm{c}}x &= V. \end{aligned} \tag{A.6}$$

From this, the natural frequency at open-circuit is:

$$\omega_{\mathrm{oc}} = \sqrt{\frac{K_{\mathrm{oc}}}{M}}. \tag{A.7}$$

Further, under static conditions $\ddot{x} = \dot{x} = 0$, Equation (A.6) reduces to

$$\begin{aligned} K_{\mathrm{oc}}x &= f \\ -K_{\mathrm{c}}x &= V. \end{aligned} \tag{A.8}$$

Equation (A.2), in the (static) blocked case, becomes

$$\begin{aligned} -K_{\mathrm{c}}Q &= f \\ \frac{1}{C_o}Q &= V, \end{aligned} \tag{A.9}$$

and by first eliminating the charge displacement from either equation, the the static blocked voltage and static blocked charge displacement are found to be:

$$V_o = \frac{f}{K_c C_o} \qquad\qquad Q_o = C_o V_o = \frac{f}{K_c}. \tag{A.10}$$

We are now in a position to write an expression for the dimensionless mechanical displacement, charge displacement, voltage, time, and natural frequency:

$$u = \frac{x}{f/K_{oc}} \qquad q = \frac{Q}{f/K_c} \qquad U = \frac{K_c C_o}{f} V \qquad \tau = \omega_{oc} t \qquad \Omega = \frac{\omega}{\omega_{oc}}. \tag{A.11}$$

The nondimensional form of the equations of motion then drops out after these quantities are substituted back into Equation (A.2):

$$\begin{aligned} u'' + 2\zeta u' + u - q &= e^{i\Omega\tau} \\ -k^2 u + q &= U. \end{aligned} \tag{A.12}$$

Derivatives with respect to the dimensionless time, τ, are denoted by primed quantities, while the modal damping ratio ζ and the electromechanical coupling coefficient k are defined as:

$$\zeta = \frac{2C}{\sqrt{K_{oc} M}} \qquad\qquad k^2 = \frac{\omega_{oc}^2 - \omega_{sc}^2}{\omega_{oc}^2} = \frac{K_{oc} - K_{sc}}{K_{oc}} = \frac{K_c^2 C_o}{K_{oc}}. \tag{A.13}$$

While not appearing explicitly in this derivation, it is important to define the dimensionless power and resistance in terms of dimensional quantities:

$$R = C_o \omega_{\mathrm{oc}} \bar{R} \qquad\qquad P = \frac{K_{\mathrm{c}} C_o}{f^2 \omega_{\mathrm{oc}}} \bar{P}. \tag{A.14}$$

Here the dimensional quantities are denoted by an overline, such as $\bar{R}$.

APPENDIX B
MATLAB CODE

B.1 Resistive Shunt

```
function dx = ode_r(t,x,zeta,a,a0,psi,ks,r)
%  ODE_R: ODE file for resistive shunt time integration
% INPUTS
%     t : current time
%     x : system state vector
%  zeta : modal damping
%     a : linear sweep rate
%    a0 : initial frequency
%   psi : initial phase
%    ks : electromechanical coupling coefficient (squared)
%     r : shunt resistance
% OUTPUT
%    dx : time derivative of the state vector, x
% USAGE
% [T,X] = ode45(@ode_r,TIME,X0,OPTIONS,Z,A,A0,PSI,KS,R);
%               where X = [x',x,q]
% EOM
%   x'' + 2 Z x' + x - q = sin(A T^2/2 + A0 T + PSI)
%        R q' - KS x + q = 0
%
dx = zeros(size(x));
dx(1) = -2*zeta*x(1)- x(2) + x(3) + sin(a/2*t^2 + a0*t + psi);
dx(2) = x(1);
dx(3) = 1/r*(ks*x(2) - x(3));
end
```

B.2 Resistive-Inductive Shunt

```
function dx = ode_rl(t,x,zeta,a,a0,psi,ks,r,l)
% ODE_RL: ODE file for resistive-inductive shunt time integration
% INPUTS
%     t : current time
%     x : system state vector
%  zeta : modal damping
%     a : linear sweep rate
%    a0 : initial frequency
```

```
%   psi : initial phase
%    ks : electromechanical coupling coefficient (squared)
%     r : shunt resistance
%     l : shunt inductance
% OUTPUT
%    dx : time derivative of the state vector, x
% USAGE
% [T,X] = ode45(@ode_rl,TIME,X0,OPTIONS,Z,A,A0,PSI,KS,R,L);
%               where X = [x',x,q',q]
% EOM
%    x'' + 2 Z x' +    x - q = sin(A T^2/2 + A0 T + PSI)
%  L q'' +   R q' - KS x + q = 0
%
    dx = zeros(size(x));
    dx(1) = -2*zeta*x(1)- x(1) + x(4) + sin(a/2*t^2 + a0*t + psi);
    dx(2) = x(1);
    dx(3) = 1/l*(-r*x(3) + ks*x(2) - x(4));
    dx(4) = x(3);
end
```

B.3 Simulation of Resonance Frequency Detuning

```
function [t_sw,E_sw,V_sw,U_max,U_env,T] = RFD_sim(t_sw,ks,zeta,a,a0,psi)
% RFD_SIM: function to simulate RFD system
% INPUTS
%   t_sw : (requested) switching time
%     ks : electromechanical coupling coefficient (squared)
%   zeta : modal damping
%      a : linear sweep rate
%     a0 : initial frequency
%    psi : initial phase
% OUTPUTS
%   t_sw : actual switch time (may not exactly equal input due to the
%                              discrete nature of the calculation)
%   E_sw : energy harvested up to the switch time
%   V_sw : voltage at the time of the switch
%  U_max : Peak response
%  U_env : response envelope at times T
```

```
%      T : integration time series

r_oc = 1E2;                     % Open-circuit shunt resistance
r_sc = 1E-2;                    % Short-circuit shunt resistance

N = 1000000;                    % Number of time steps for integration
X0 = [0 0 0];                   % Initial condtions
T = linspace(0,2/a,N);          % Time span for integration
T_OC = T(T<t_sw);               % OC time span
T_SC = T(T>t_sw);               % SC time span

% Simulate at open-circuit
[t_oc,x_oc] = ode45(ode_r,T_OC,X0,zeta,a,a0,psi,ks,r_oc);

X0 = x_oc(end,:); % set intitial condition for sc integration

% Simulate at short-circuit
[t_sc,x_sc] = ode45(ode_r,T_SC,X0,zeta,a,a0,psi,ks,r_sc);

T = zeros(N-1,1);
T = [t_oc' t_sc(2:end)'];
X = [x_oc' x_sc(2:end,:)'];

% Displacement, Charge displacement:
u = X(2,:);
q = X(3,:);

dt = diff(T);

% Voltage, Power:
V = (ks*u-q);
P_oc = V(T<t_sw).^2/r_oc;
P_sc = V(T>t_sw).^2/r_sc;
P = [P_oc P_sc];

% Energy:
E = zeros(length(T),1);
for i = 2:length(T)
    E(i) = E(i-1) + P(i-1)*dt(i-1);
end
% Find energy harvested up to switching time:
t_temp = T(T<t_sw);
```

```
t_sw = t_temp(end);
E_sw = E(T==t_sw);
V_sw = V(T==t_sw);

% Response Envelope
[tu_temp,U_temp] = peakpick(T,u,0);
U_env = interp1(tu_temp,U_temp,T,'spline');

% Peak Response:
U_max = max(U_env);
end
```

LIST OF REFERENCES

[1] E. Poursaeidi and H. Bakhtiari, "Fatigue growth simulation in a first stage of compressor blade," *Engineering Failure Analysis*, vol. 45, pp. 314–325, 2014.

[2] F. Mohammadi, A. Khan, and R. B. Cass, "Power generation from piezoelectric lead zirconate titanate fiber composites," in *Symposium D – Electronics on Unconventional Substrates – Electrotextiles and Giant-Area Flexible Circuits*, ser. MRS Proceedings, vol. 736. Boston, MA: MRS, 1 2002, MRS 736.

[3] Y. C. Shu and I. C. Lien, "Analysis of power output for piezoelectric energy harvesting systems," *Smart Materials and Structures*, vol. 15, no. 6, pp. 1499–1512, Aug. 2006.

[4] U. Aridogan, I. Basdogan, and A. Erturk, "Broadband and band-limited random vibration energy harvesting using a piezoelectric patch on a thin plate," in *Proceedings of SPIE Smart Structures / NDE 2014*. San Diego, CA: SPIE, 2014, SPIE 9057 – 10.

[5] J. A. Paradiso and T. Starner, "Energy scavenging for mobile and wireless electronics," *IEEE Pervasive Computing*, vol. 4, no. 1, pp. 18–27, Mar. 2005.

[6] "Piezoelectric ceramics: Properties and applications," Pointwise, Inc., Gridgen, Fort Worth, Texas, 2005. [Online]. Available: http://www.pointwise.com/images/app_turbo_aachen_1000px.png

[7] M. N. V. Ramesh and N. M. Rao, "Free vibration analysis of rotating functionally-graded cantilever beams," *International Journal of Acoustics and Vibrations*, vol. 19, no. 1, pp. 31–41, Mar. 2014.

[8] J. L. Kauffman and G. A. Lesieutre, "Piezoelectric-based vibration reduction of turbomachinery bladed disks via resonance frequency detuning," *AIAA Journal*, vol. 50, no. 5, pp. 1137–1144, May 2012.

[9] A. T. S. Bureau, "Engine failure, vh-sba wagga wagga aerodrome, new south wales, 4 october 2009," ATSB Transport Safety Report AO-2009-061, November 2010.

[10] AgentJayZ. (2011) J47 ceramic blades - turbine engines: A closer look. Still image from YouTube video: https://www.youtube.com/watch?v=1Vzbd3kO7kU. [Online]. Available: http://i.ytimg.com/vi/1Vzbd3kO7kU/maxresdefault.jpg

[11] O. Cleynen. (2013) Compressor blisk on display. File: Compressor blisk on display (4).jpg. [Online]. Available: https://commons.wikimedia.org/wiki/File:Compressor_blisk_on_display_(4).jpg

[12] E. M. K. Jr., "Damping of flexural waves by a constrained viscoelastic layer," *Journal of the Acoustical Society of America*, vol. 31, no. 7, pp. 952–962, 1959.

[13] J. L. Kauffman, "Vibration reduction of integrally bladed rotors using piezoelectric materials," Ph.D. dissertation, Pennsylvania Statue University, 2012.

[14] N. W. Hagood and A. von Flatow, "Damping of structural vibrations with piezoelectric materials and passive electrical networks," *Journal of Sound and Vibration*, vol. 146, no. 2, pp. 243–268, Apr. 1991.

[15] R. Forward, "Electronic damping of vibrations in optical structures," *Journal of Sound and Vibration*, vol. 18, no. 5, pp. 690–697, 1979.

[16] W. W. Clark, "Vibration control with state-switched piezoelectric materials," *Journal of Intelligent Material Systems and Structures*, vol. 11, no. 4, pp. 263–271, 2000.

[17] W. P. Mason, "Piezoelectricity, its history and applications," *The Journal of the Acoustical Society of America*, vol. 20, no. 5, pp. 1561–1566, Dec. 1981.

[18] S. Datta. (2014) Piezoelectric materials: Crystal orientation and poling direction. [Online]. Available: http://www.comsol.com/blogs/piezoelectric-materials-crystal-orientation-poling-direction

[19] Anon, "Piezoelectric ceramics: Properties and applications," Philips Components, Philips Components, 1991.

[20] Institute of Electrical and Electronics Engineers, "*IEEE* standard on piezoelectricity," ANSI/IEEE Std. 176-1987, IEEE, New York, NY, IEEE, New York, NY, 1987.

[21] T. D. Hynds and J. L. Kauffman, "Harvesting at the margins: A study of energy harvesting away from optimal conditions," in *Proceedings of AIAA SciTech 2015*. Orlando, FL: AIAA, 2015, AIAA.

[22] S. Zhang, R. Xia, L. Lebrun, D. Anderson, and T. R. Shrout, "Piezoelectric materials for high power, high temperature applications," *Material Letters*, vol. 59, no. 27, pp. 3471–3475, 2005.

[23] H. A. Sodano, D. J. Inman, and G. Park, "Generation and storage of electricity from power harvesting devices," *Journal of Intelligent Material Systems and Structures*, vol. 16, no. 1, pp. 67–75, Jan 2005.

[24] H. Sato, Y. Shimojo, and T. Sekiya, "Lead zirconate titanate fiber, smart board using lead zirconate titanate fiber, actuator utilizing smart board, and sensor utilizing smart board," Jul. 31 2003, U.S. Patent App. 10/347,248. [Online]. Available: https://www.google.com.ar/patents/US20030141785

[25] X. Chen and Y. Shi, "Selected topics in micro/nano-robotics for biomedical applications: Pzt nano active fiber composites-based acoustic emission sensor," Springer-Verlag, New York, NY, pp. 9–22, 2013.

[26] T. A. Anderson and D. W. Sexton, "A vibration energy harvesting sensor platform for increased industrial efficiency," in *Proceedings of SPIE Smart Structures and Materials: Sensors and Smart Structures Technologies for Civil, Mechanical, and Aerospace Systems*. San Diego, CA: SPIE, 2006, SPIE Vol. 6174.

[27] S. Jiang, X. Li, S. Guo, Y. Hu, J. Yang, and Q. Jiang, "Performance of a piezoelectric bimorph for scavenging vibration energy," *Smart Materials and Structures*, vol. 14, no. 4, p. 769, July 2005.

[28] C. W. S. To, "Vibration of a cantilever beam with a base excitation and tip mass," *Journal of Sound and Vibration*, vol. 83, no. 4, pp. 445–460, Aug. 1982.

[29] J. M. Renno, M. F. Daqaq, and D. J. Inman, "On the optimal energy harvesting from a vibration source," *Journal of Sound and Vibration*, vol. 320, no. 1–2, pp. 386–405, Aug.–Sept. 2009.

[30] A. Badel, D. Guyomar, E. Lefeuvre, and C. Richard, "Piezoelectric energy harvesting using a synchronized switch technique," *Journal of Intelligent Material Systems and Structures*, vol. 17, no. 8–9, pp. 831–839, Aug.–Sept. 2006.

[31] D. Guyomar, A. Badel, E. Lefeuvre, and C. Richard, "Toward energy harvesting using piezoelectric materials and conversion improvement by nonlinear processing," *IEEE Transactions on Ultrasonics, Ferroelectrics, and Frequency Control*, vol. 52, no. 4, pp. 584–595, Aug. 2005.

[32] G. A. Lesieutre, G. K. Ottman, and H. F. Hofmann, "Damping as a result of piezoelectric energy harvesting," *Journal of Sound and Vibration*, vol. 269, pp. 991–1001, 2004.

[33] C. Richard, D. Guyomar, D. Audigier, and G. Ching, "Semi-passive damping using continuous switching of a piezoelectric device," in *Proceedings of SPIE Conference on Passive Damping and Isolation*. Newport Beach, CA: SPIE, 1999, SPIE 3672, pp. 104–111.

[34] C. Richard, D. Guyomar, D. Audigier, and H. Bassaler, "Semi-passive damping using continuous switching of a piezoelectric device," in *Proceedings of SPIE Smart Structures and Materials 2000: Damping and Isolation*. SPIE, 2000, SPIE 3989, pp. 288–299.

[35] J. L. Kauffman and G. A. Lesieutre, "Piezoeletric-based vibration dampig and control of turbomachinery bladed disks," in *Proceedings of* 21st *ICAST*, 2010.

[36] ——, "Performance of piezoelectric-based damping techniques for structures with changing excitation frequencies," in *Proceedings of SPIE Smart Structures / NDE 2011*. San Diego, CA: SPIE, 2011, SPIE 7977–12.

[37] ——, "A low-order model for the design of piezoelectric energy harvesting devices," *Journal of Intelligent Material Systems and Structures*, vol. 70, no. 6, pp. 495–504, Mar. 2009.

[38] G. K. Lopp and J. L. Kauffman, "Switch triggers for optimal vibration reduction via resonance frequency detuning," in *Proceedings of ASME Turbo Expo 2014*. D*ü*sseldorf, GE: ASME, 2014, ASME GT2014-27263.

[39] R. Markert and M. Siedler, "Analytically based estimation of the maximum amplitude during passage through resonance," *International Journal of Solids and Structures*, vol. 38, no. 2, pp. 1975–1992, 2001.